Oil slicks in the Gulf of Guinea - 10 years of Envisat ASAR observations

Zhour Najoui [a], Nellya Amoussou [c], Serge Riazanoff [a,b], Guillaume Aurel [a], Frédéric Frappart[d]

[a] *VisioTerra, 14 rue Albert Einstein Champs-sur-Marne, France, zhour.najoui-nafai@visioterra.fr, serge.riazanoff@visioterra.fr, guillaume.aurel@visioterra.fr.*

[b] *Université Gustave Eiffel – Institut Gaspard Monge -IGM, 5 boulevard Descartes, Champs sur Marne, serge.riazanoff@visioterra.fr.*

[c] *Sorbonne Université - Laboratoire d'Océanographie et du Climat : Expérimentations et Approches Numériques (LOCEAN), 4 Place Jussieu, 75005 Paris, lydieamoussou14@gmail.com.*

[d] *INRAE, ISPA, UMR 1391 INRAE/Bordeaux Sciences Agro, Villenave d'Ornon, France, frederic.frappart@inrae.fr.*

Correspondence to: Zhour NAJOUI (zhour.najoui-nafai@visioterra.fr)

1. Abstract

The Gulf of Guinea is a very active area regarding maritime traffic as well as oil and gas exploitation. Due to some actors failure to comply with environmental standards, this region has been subject to a large number of oil pollution. This pollution comes in addition to natural oil seepages from the ocean floor. This study aims to detect oil slicks spilled in the Gulf of Guinea and analyse their spatial distribution using Synthetic Aperture Radar (SAR) images. The previous works have already locally mapped oil slicks in this area, this study proves to be the first one to achieve a global statistical analysis based on 10 years of radar images covering 17 Exclusive Economic Zones of the Gulf of Guinea. The present study has been based on a database of 3,644 SAR images, collected between 2002 and 2012 by the Advanced SAR (ASAR) sensor onboard the European Spatial Agency (ESA) Envisat mission, which allowed the identification of 18,063 oil slicks. These "Oil slicks" herein detected encompass: -"oil spills" of anthropogenic origin and - "oil seeps" of natural origin (natural oil reservoir leaks).

2. Introduction

The Deep Water Horizon (DWH) disaster that occurred on April 20, 2010 in the Gulf of Mexico aroused worldwide outrage both for its human and environmental impacts (Leifer et al., 2012). There was great interest of the public, media, politicians and scientists characterized by a meticulous follow-up of the progression of the oil slicks (Caruso et al., 2013; Pinkston and Flemings, 2019). And yet, a disaster similar to that of the DWH would not be surprising along the African coast and, in particular, in the Gulf of Guinea, where recurrent oil spills are observed. These may be caused by deballasting operations (Albakjaji, 2010) and releases due to shipwrecks (Fuhrer, 2012).

If oil constitutes an important resource for the countries of the Gulf of Guinea from an economic point of view (Ovadia, 2016), the environmental impact caused by the frequent oil spills has provoked serious negative effects on both the environment and the local economy (Jafarzadeh et al., 2021; Okafor-Yarwood, 2018; Yaghmour et al., 2022). The weakness of national monitoring and legislation control is likely to limit the compliance to the major standards followed by large companies. Thus, the provision of observation tools that can enable people of Africa to ensure good monitoring and better management of the Gulf of Guinea is necessary. This facility is to enable African countries to monitor offshore oil exploitation concessions using free data provided by ESA and now the European Union (EU) in the framework of the Copernicus programme.

Synthetic Aperture Radar (SAR) images have proven to be a useful tool for oil slicks mapping due to the dampening effect that oil has on capillary and small gravity waves, called Bragg waves. The latter are generated on water by local winds and they are responsible for the radar backscattering (Gade et al., 1998; Jackson et al., 2004; Mercier and Girard-Ardhuin, 2006; Shu et al., 2010; Xu et al., 2015). As a consequence, oil slicks appear darker compared to nearby undampened water surface where Bragg waves produce brighter radar backscattering. In addition, long-term time-series of radar images are freely available since 1991 (ERS-1 mission was launched in 1991, ERS-2 in 1995, Envisat in 2002, Sentinel-1a in 2014 and Sentinel-1b in 2016) while near real time radar images are foreseen to be freely available at least until 2030 owing to Sentinel constellation. This data availability allows extensive studies of past and future pollution as well as operational detection of oil slicks using satellite radar imagery (Kubat et al., 1998).

In this study, SAR images acquired by the European Spatial Agency (ESA) mission Envisat has been used. Envisat was launched on March 1, 2002, its payload contained ten instruments. The Advanced Synthetic Aperture Radar (ASAR) sensor onboard is the second generation of SAR instrument developed by ESA , (Louet and Bruzzi, 1999). Envisat nominal life (5 years) has been doubled until the loss of the satellite on April 8, 2012 (10 years).

The Gulf of Guinea is now one of the largest oil producing regions of the world and yet, very few studies have really analysed its situation regarding oil slicks (both spills and seeps). The present study focuses on the spatial distribution of the oil slicks occurring from 2002 to 2012 by Exclusive Economic Zone (EEZ) throughout the Gulf of Guinea using Envisat ASAR radar images.

3. Presentation of the study area

3.1. Geographic location

The radar images used in this study were acquired over the Gulf of Guinea. This region is located in the Atlantic Ocean in the southwest of Africa. According to the International Hydrographic Organization (Bassou, 2016), it extends from Guinea Bissau to Angola and covers the EEZ of 16 countries bordering the coast (extending over 7000 km): Guinea Bissau (GNB), Guinea Conakry (GIN), Sierra Leone (SLE), Liberia (LBR), Ivory Coast (CIV), Ghana (GHA), Togo (TGO), Benin (BEN), Nigeria (NGA), Cameroon (CMR), Equatorial Guinea (GNQ), Sao Tome and Principe (STP), Gabon (GAB), Republic of Congo (COG), Democratic Republic of Congo (COD), and Angola (AGO) (fig. 1).

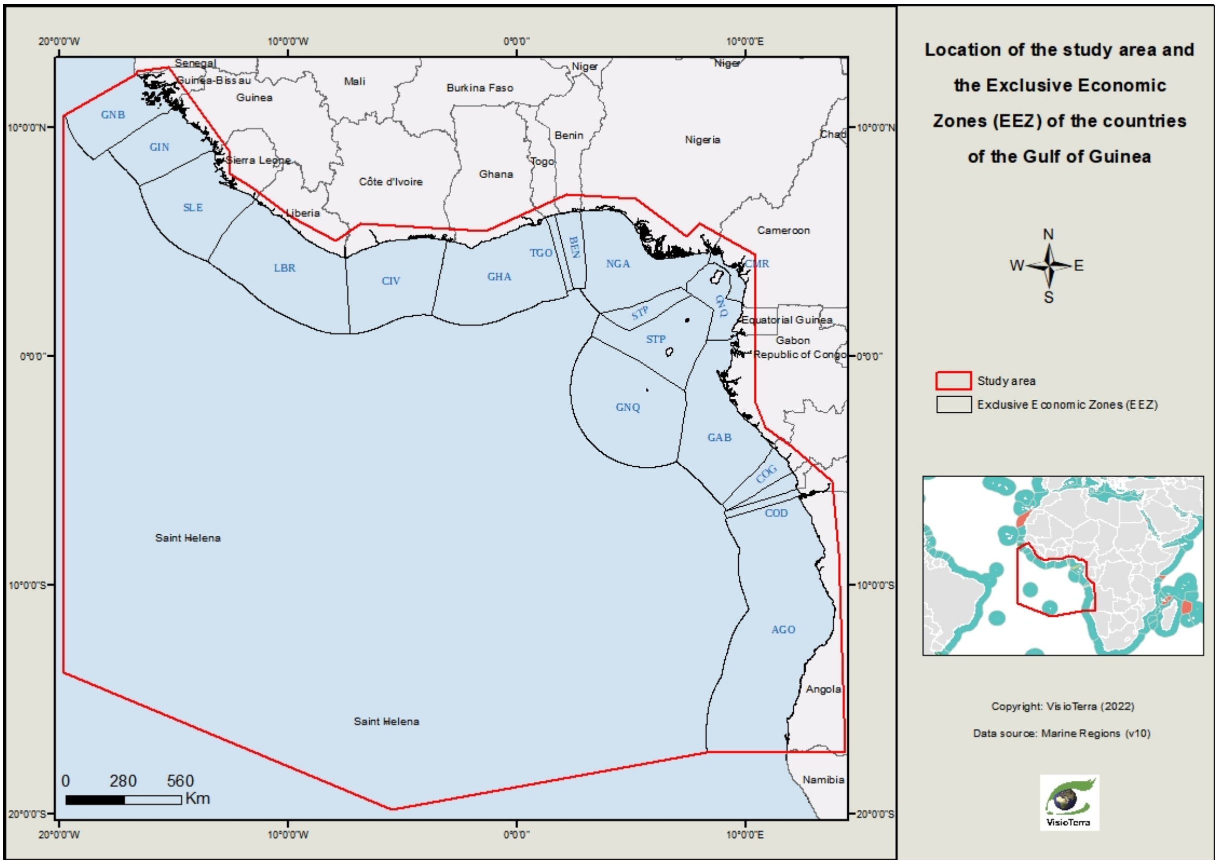

fig. 1 - Location of the study area in the Gulf of Guinea and the Exclusive Economic Zones of the different countries.

3.2. Geological location

Petroleum is a natural mixture composed mainly of hydrocarbons. It is formed within certain sedimentary rocks by transformation of organic matter (plankton, plants, animals, etc.) incorporated into the deposit. It is a slow and gradual process occurring in a sedimentary basin.

Indeed, the transformation of organic matter into oil spans millions of years, and has been punctuated by several stages including the formation of an intermediate substance called kerogen. A given layer of sediment sinks and is buried under other layers of sediment. Depending on the filling of the basin, the heat flow and pressure induced by geologic processes, organic matter may change from kerogen to petroleum. Oil being less dense than water, it tends to migrate to the upper layers of the sedimentary strata. These sedimentary strata have a certain geometric configuration defined by the tectonic structure of the basin. During this structuring, different areas may have risen higher (anticlines) or have sunk lower (synclines) relatively to the rest of the stratum. When these upper zones are topped by a cover allowing the oil to escape through faults or fractures, they constitute oil deposits exploited nowadays in offshore or onshore areas.

The Gulf of Guinea is located in a passive zone resulting from the opening of the South Atlantic Ocean initiated during the Lower Cretaceous, breaking up south-west Gondwana. The climate during this period was hot, humid and stable, which favours chemical weathering of the mainland. Eroded material brought chemical elements to the Gulf of Guinea; in particular, the Niger Delta transported sediments rich in hydrocarbons. These numerous characteristics make this area a source of natural seepages also called oil seeps (Lawrence et al., 2002)

3.3. Oil exploration in the Gulf of Guinea

The Gulf of Guinea region has entered the global oil landscape comparatively quite recently. In 1982, the signing of the Montego Bay convention extended the maritime territories of riparian countries over their EEZ, 200 nautical miles ($\approx$ 370 km) off their coasts, which encouraged offshore exploration (Bassou 2016). The Gulf of Guinea is now one of the largest oil producing regions in the world.

Indeed, since the installation of its first oil platforms (anchored and floating platforms) between 1960 and 1970 (Favennec et al., 2003), the Gulf of Guinea has become one of the favourite destinations of international oil investors (Tull, 2008). The good quality of its oil justifies the ~~attractiveness~~ of foreign countries to the region (Ngodi, 2005). Since the 2000s, it has supplied more than 55 billion barrels, i.e. 5% of world oil production (Mfewou et al., 2018) and 60% of total daily crude oil production in sub-Saharan Africa. Offshore is the default mode of oil extraction in the Gulf of Guinea (Favennec et al., 2003). The depletion of coastal water resources (shallow water; $\leq$ 200 m) means that the relative share of deep water exploration (Deep water; 450 m - 1800 m), or even in ultra-deep water (1800 m - 3000 m) is increasing. This is the case, for example, off the coast of Angola or Gabon.

3.4. Oil pollution and environmental impacts

The Gulf of Guinea is a very active area in oil exploration. The oil spills found in the region are unparalleled in frequency and their toxicity induces serious repercussions both on the marine environment and on the ecosystem (Bagby et al., 2017; Chalghmi, 2015; Khanna et al., 2018; Langangen et al., 2017; Li et al., 2019; Li and Johnson, 2019; NAE-NRC, 2012; Reuscher et al., 2020).

Several cases of accidents caused by the exploitation of offshore oil are documented. Apart from that, several accidents have occurred following the exploitation of offshore oil fields. The frequency of oil spills in the Gulf of Guinea is said to be due, among other factors to oil production operations, inadequate production equipment leading to corrosion of pipelines and tanks, to disasters, sabotage and vandalism (Adelana and Adeosun, 2011).

Environmental consequences include the loss of habitat for corals and seagrass, the destruction of flora (reduction of mangroves and certain species of algae) and that fauna (extinction of sea turtles) (Scheren et al., 2002). Oil slicks have a devastating effect on fishing activity. Many Nigerian fishermen can no longer practice their profession, especially off the Niger Delta.

4. Dataset and Method

4.1. Radar data

Several spaceborne SAR systems have been widely used for marine pollution monitoring and mapping (Brekke and Solberg, 2008; Del Frate et al., 2000; Dong et al., 2022; Espedal, 1999; Fiscella et al., 2000; Gade et al., 1998; Garcia-Pineda et al., 2008; Kanaa et al., 2003; Li and Johnson, 2019; Liu et al., 1997; Marghany, 2015; Solberg et al., 1999; Suresh et al., 2015). In this study, we used SAR images acquired by Envisat ASAR from 2002 to 2012. Envisat ASAR operated at the radar frequency of 5.331 GHz in C-Band (4.20 – 5.75 GHz) in various modes including WSM (Wide Swath Medium-resolution). WSM ASAR images were acquired along swaths 400 km wide at a spatial resolution of approximately 150 m by 150 m. WSM products are delivered with a ground pixel spacing of 75 m by 75 m. Envisat ASAR operated in one of two polarizations types, either HH (horizontal transmission / horizontal reception) or VV (vertical transmission / vertical reception). ASAR WSM operated according to the ScanSAR principle, using five predetermined overlapping antenna beams (also called subswaths) which covered the wide swath. The ScanSAR principle consists in achieving swath widening by the use of an antenna beam which is electronically steerable in elevation (Miranda et al., 2013).

On a radar image, the areas covered by oil appear as smooth dark regions with low backscattering. This is due to the damping effect that the oil produces on capillary waves and small waves of gravity. On a oil-free surface, a significant part of the energy will be backscattered towards the radar making it appear lighter (Alpers et al., 2017). The backscatter of the radar signal is also influenced by environmental conditions such as: wind speed and sea state (Fingas and Brown, 2017; Zhang et al., 2014). The ideal wind speed for the detection of oil slicks is in an interval that depends on the authors: - 2 m/s to 10 m/s (MacDonald et al., 2015), -1.5 m/s to 6.5 m/s (Jatiault et al., 2017), -2.09 m/s to 8.33 m/s (Najoui, 2017)... Vertical polarization (VV) is the most effective mode for detecting oil spills on the sea surface (Brekke and Solberg, 2008; Jatiault et al., 2017; Najoui et al., 2018a, 2018b).

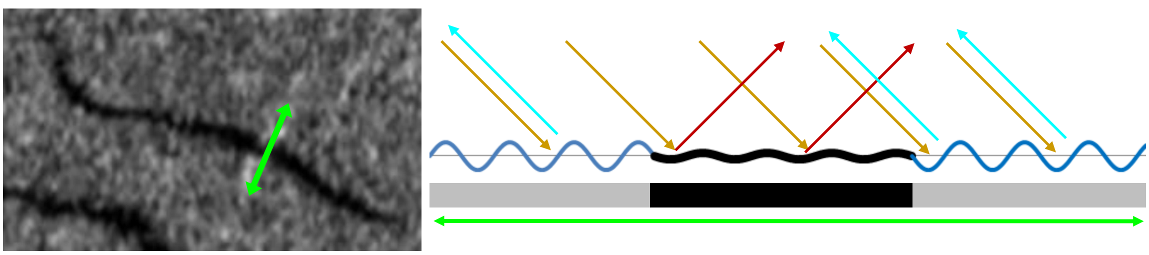

fig. 2 - Backscattering of the radar signal in the presence and absence of oil (Najoui, 2017).

All the Envisat ASAR WSM scenes available in the study area have been processed leading to an amount of **3,644** scenes after eliminating redundant products. The fig. 3 illustrates the spatial distribution of the occurrences of Envisat ASAR WSM observations between 2002 and 2012 in the Gulf of Guinea. The number of WSM observations is noticeably higher near the coasts.

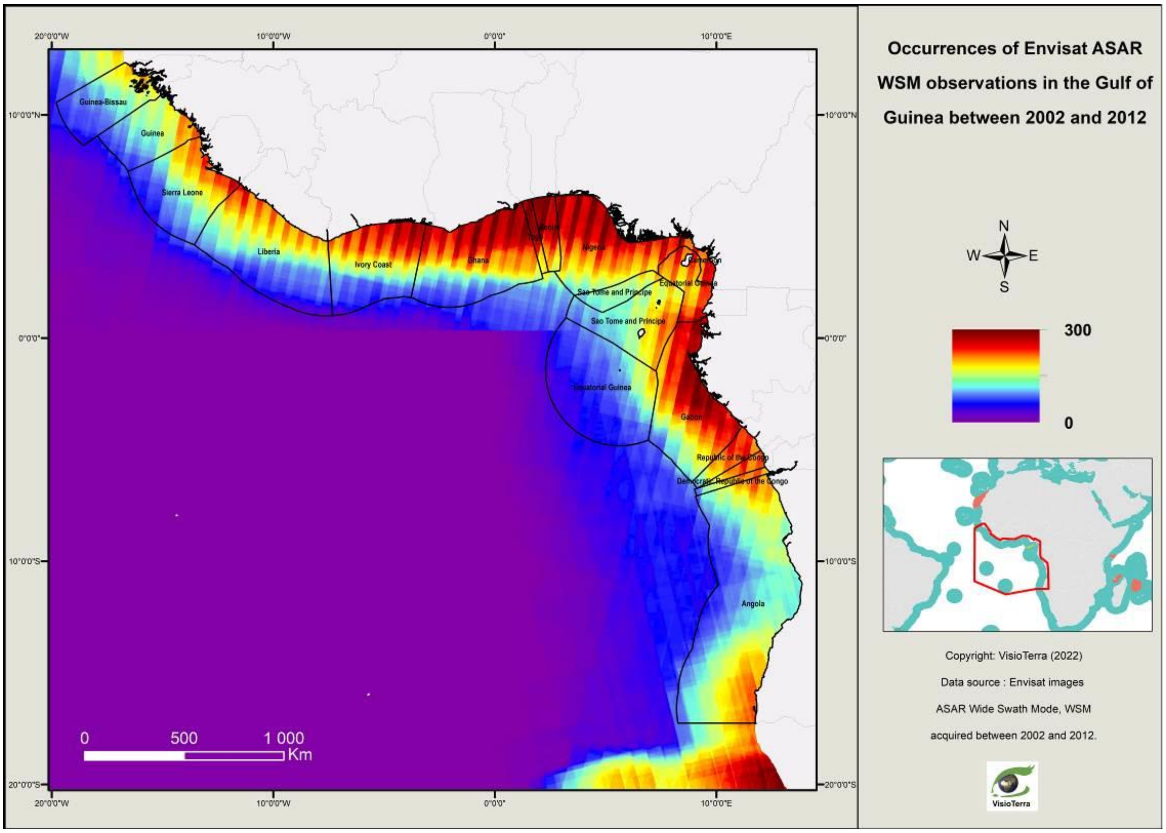

fig. 3 - Occurrences of Envisat ASAR WSM observations between 2002 and 2012.

4.2. Image preprocessing

The database of 3,644 images has been georeferenced in the geographic coordinate reference system over the WGS84 ellipsoid, datum WGS84. A land mask has been applied and the images have been radiometrically corrected. The radiometric correction consists in correcting the brightness variations due to SAR peculiarities. Indeed, the radar backscattering on the offshore area is dominated by non-Lambertian reflections (the surface does not reflect the radiation uniformly in all directions). This non-Lambertian reflection leads to heterogeneity of the brightness in the radar image: brighter along the near-range (closest to the NADIR line) and darker along the far-range. The input images have a 16-bits Digital Number (DN) dynamic which requires reduction to 8-bits to be displayable on a usual screen. The applied preprocessing consists in applying a local stretching with an average of 140 and a standard deviation of 60 on a sliding window of 301 pixels in order to optimize the detectability of the oil slicks (fig. 4) (Najoui, 2017; Najoui et al., 2018b).

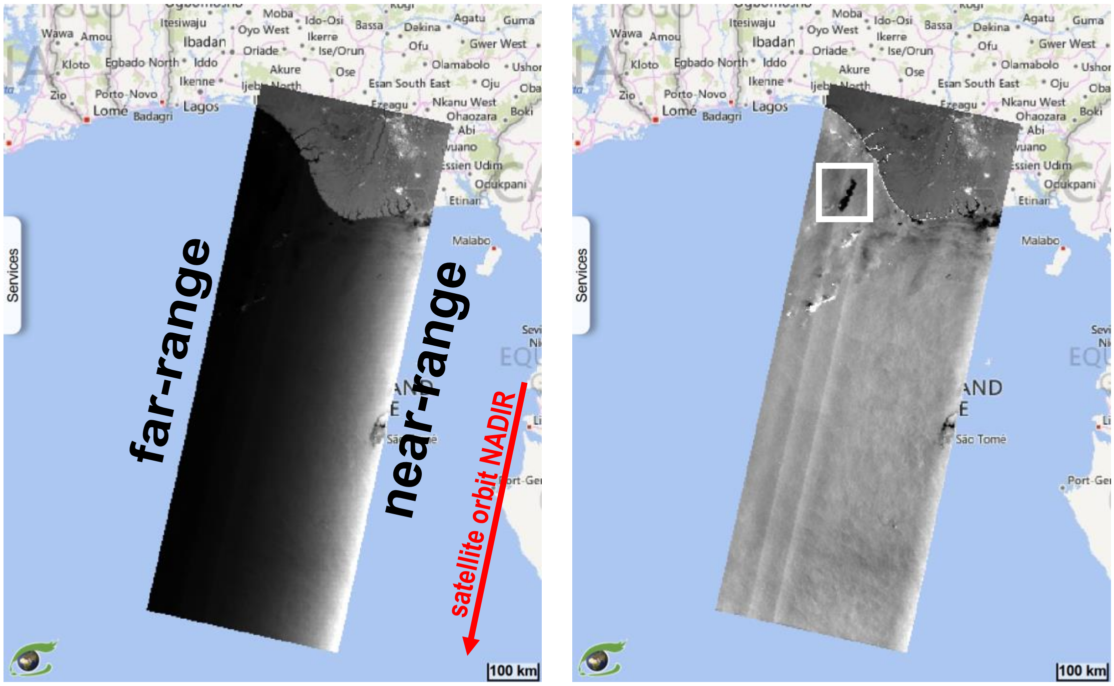

fig. 4 - ASAR WSM images (21/12/2011) before (left) and after (right) local stretching showing a leak from an oil platform (see fig. 5).

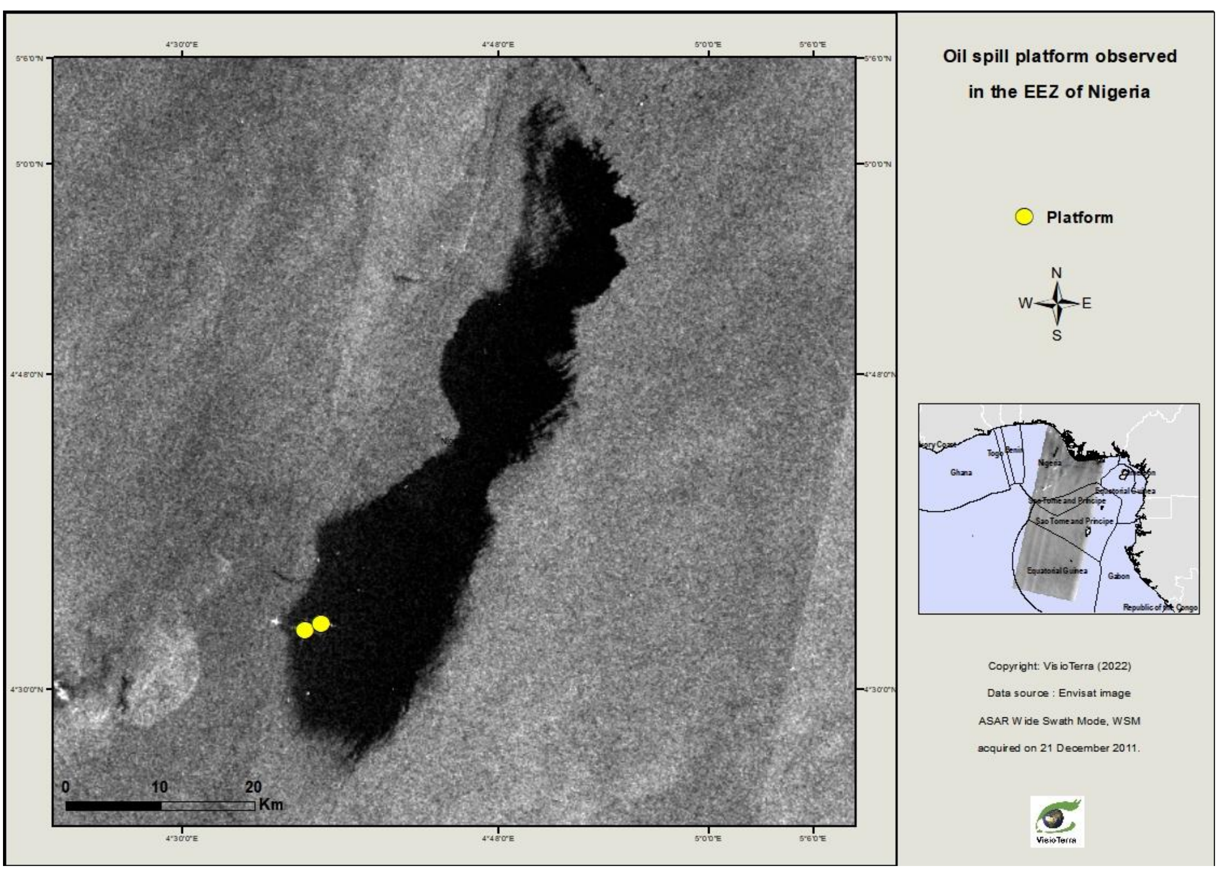

fig. 5 - Oil spill platform observed in the EEZ of Nigeria (21/12/2011). The platforms are represented by the yellow dots (see hyperlook http://visioterra.org/VtWeb/hyperlook/504c7208cc184c12b42ed036bc9912f3).

4.3. Manual detection

Oil slicks appear as dark patches on radar images because they flatten the surface of the sea. However, in addition to oil slicks, many phenomena also may appear as dark. Non-oil dark patches are termed as look-alikes features that include upwelling, eddies, rainfalls, wind shadows, bathymetry, internal waves, current shear zones, etc. (Brekke and Solberg, 2005; Espedal, 1999; Xu et al., 2015).

The detection of oil slicks has been performed using a reliable manual detection approach as explained in (Najoui et al., 2018a, Jackson et al., 2004). In fact, the 3,644 radar images used in this publication have been manually interpreted. The detection of oil slicks and their categorisation were carried out following three stages of analysis: 1) interpretation based on morphological and textural criteria, 2) multi-date analysis of repetitive oil slicks, and 3) validation using auxiliary data.

According to the morphological and textural criteria oil slicks may be subdivided into two major classes: biogenic and mineral. Biogenic oil slicks are organic films made of substances produced by plankton and other marine organisms. The mineral oil slicks can be subdivided between natural seeps (fig. 6), emitted naturally from the sea bottom, and anthropogenic oil spills that originate from ships (fig. 7), refineries, oil terminals, industrial plants, oil platforms (fig. 8) and pipelines (Espedal, 1999). For instance, oil spills from platforms or ships induce significant slicks (Johannessen et al., 2000; Leifer et al., 2012; Trivero and Biamino, 2010). If biogenic oil slicks appear as shiny diffracting points on SAR data, oil seeps are characterized by curvilinear shapes due to short-term changes of the strength and orientation of the wind and of the surface currents (Espedal, 1999).

Thereafter, a multi-date analysis has been performed. We use all the interpretations at different dates in order to assess the manual interpretation. Indeed, repetitive slicks are, more likely, due to leaks from static sources: a geological feature for oil seeps, a platform or pipeline for oil spills, for instance. The shape of these oil slicks from static sources is induced by the strength and orientation of the short-term changes of both wind and sea surface current. Usually, this type of slicks from natural oil seeps and oil spills from oil platforms constitutes forms of "astroseeps" or "flower structures" (fig. 9). In general, ships that discharge oily effluents do it ~~in~~ route, leaving behind them linear-shaped spills or trails. When oil is discharged in a current-free and calm sea, the resulting overall spill geometry will follow the route of the ship. This linearity is used to identify such oil spills. However, when a deballasting ship maneuvers or when a non-uniform surface current is present, then, the contour of the spill can deviate significantly from linearity. When oil is discharged from a moving ship, it also spreads laterally, resulting in oil trail which width increases with distance from the ship. In many cases, a white dot ahead of the deballasting testifies to the metal structure of the ship and the size, or even the shape, of the dot can be an indicator of the size of the vessel.

Finally, the validation of the analysis has been performed by the integration of the manual detection output in a Geographic Information System (GIS) with other auxiliary data. These auxiliary data include the location of oil platforms, oil and gas fields, available bathymetric, geological and structural data, marine traffic, wind and current field direction… This work has led to ~~the constitution of~~ a dataset with 18,063 interpreted oil slicks (Najoui, 2022).

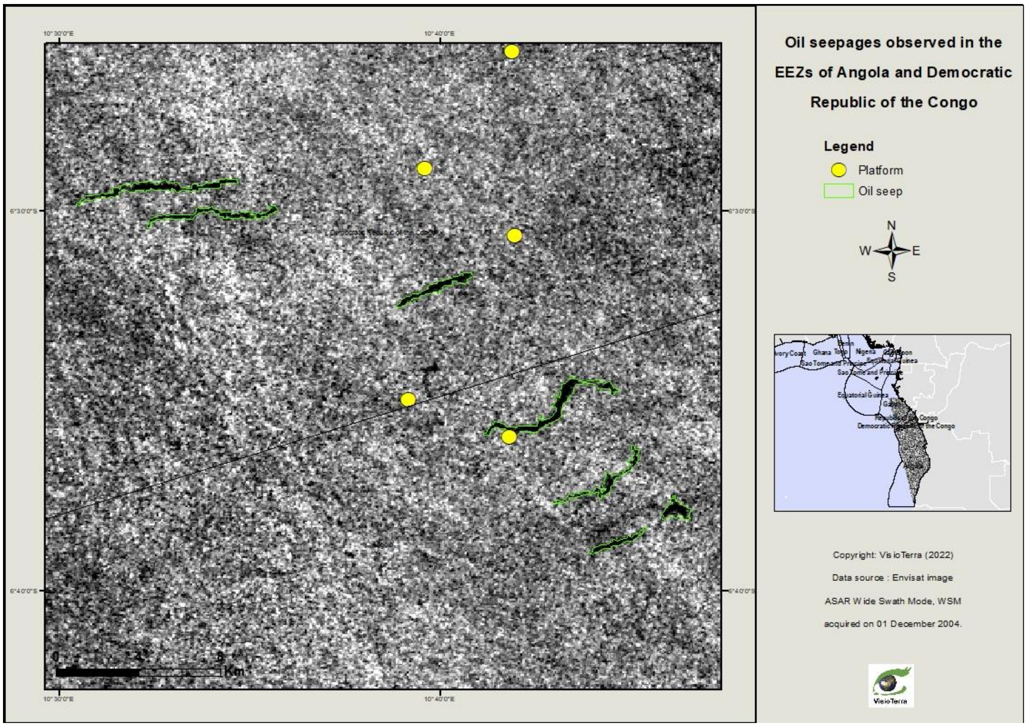

fig. 6 - Oil seeps (1st December 2004) observed in the EEZ of Angola and Democratic Republic of the Congo. The platforms are represented by the yellow dots.

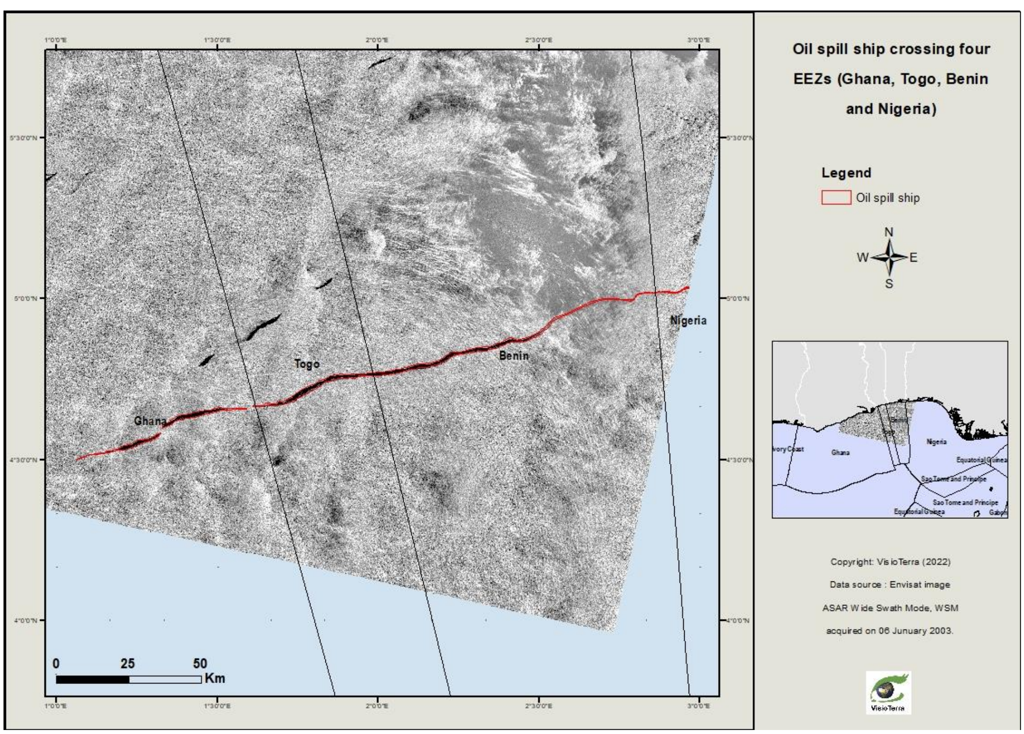

fig. 7 - Oil spill ship (5 January 2003) crossing four EEZs (Ghana, Togo, Benin and Nigeria).

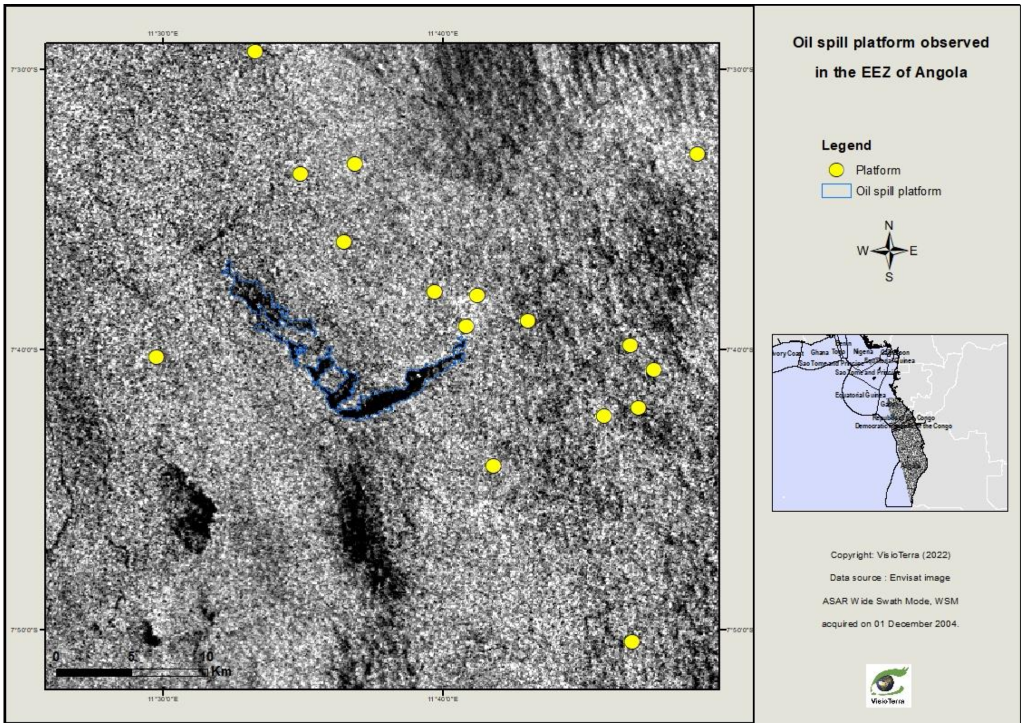

fig. 8 - Oil spill platform (1st December 2004) observed in the EEZ of Angola. The platforms are represented by the yellow dots.

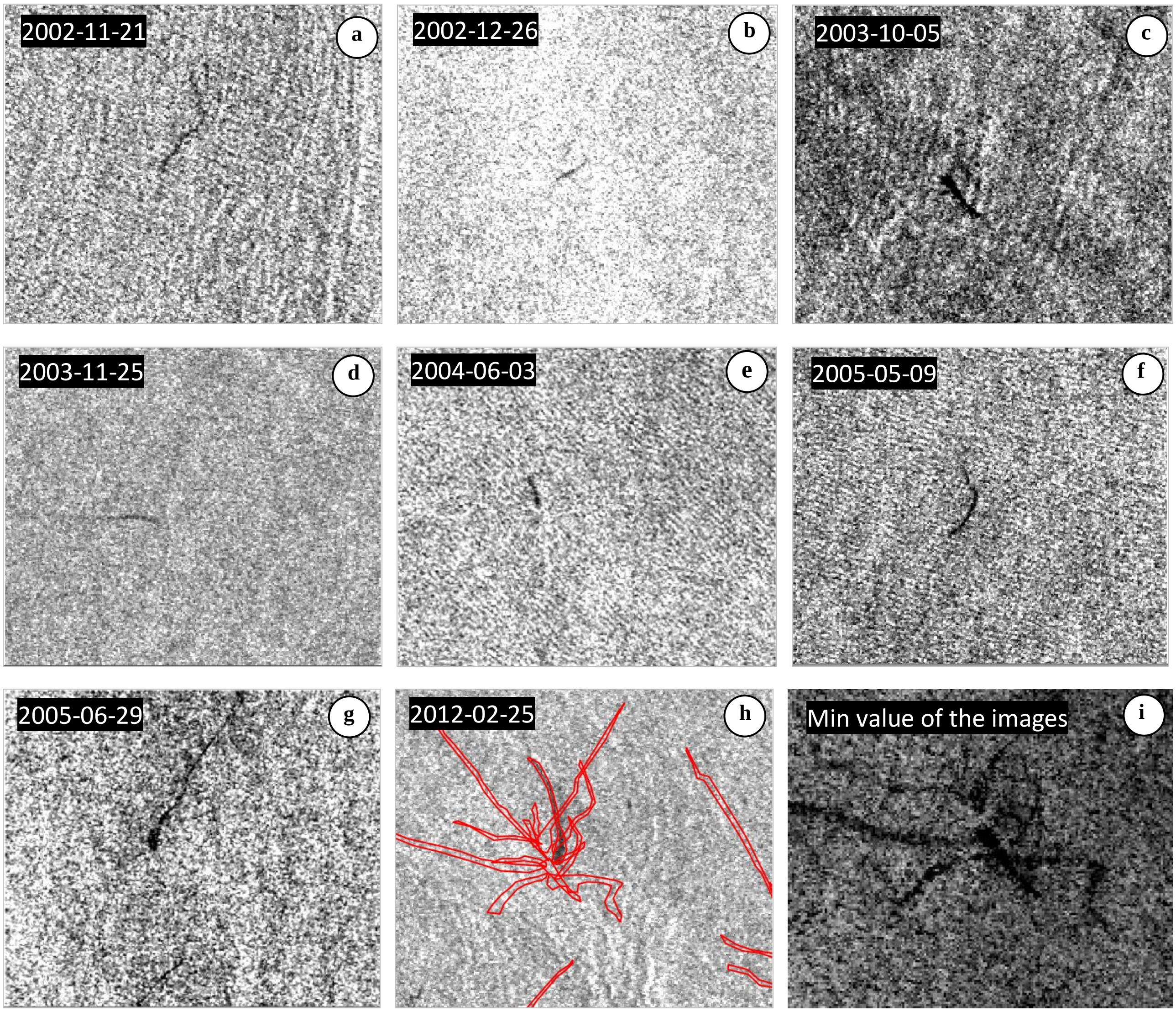

fig. 9 - Example of multitemporal analysis with astroseeps structure observed in the Lower Congo basin. Images a, b, c, d, e, f and g are Envisat ASAR images acquired at different dates with observed seeps. Image h shows an Envisat ASAR image with interpreted seeps. Image i shows the Envisat ASAR minimum image (i.e. each pixel is the minimum observed for the 7 dates) with an "astroseep" structure.

4.4. Mean area covered in oil

The image-interpretation described in the previous section results in the delimitation of closed polygons corresponding to the oil slicks. These polygons are "embedded" in a raster image to perform the statistical study. Since each location within the area of interest has not been observed an equal number of times by the Envisat satellite, an "observation occurrence map" has been produced (fig. 3). In fact, each location has not been equally observed because of the partial overlap of neighbouring swaths and the use of both ascending and descending orbits. Hence, it was necessary to locally normalize the oil slicks number distribution by dividing the number of oil slick occurrences by the number of observations made by Envisat ASAR over the study area which gives the relative frequency of the presence of oil per pixel.

The **probability of presence of oil X per pixel (P_X(l,p))** is equal to the number of occurrences of oil X in a pixel (S_X(l,p)) divided by the number of observations (O(l,p)) of the same pixel (eq.1).

$$P_X(l,p) = \frac{S_X(l,p)}{O(l,p)} \qquad \text{(eq. 1)}$$

Where :

- $S_X(l,p)$ is the number of occurrences of the presence of oil X detected on a pixel by image-interpretation,
- X is the type of oil. It can be natural leaks (oil seepages), pollution by boats (oil spill ships) and pollution by platforms (oil spill platforms),
- (l,p) are the coordinates (l, p) of the current pixel representing the rows and columns of the image,
- O(l,p) are the number of observations as they appear in the footprints of the processed images Envisat ASAR WSM,
- $P_X(l,p)$ is the normalized occurrence also called probability of oil presence at pixel (l, p).

For each class X of oil slick among (e) “seepage”, (s) “spill from ship”, and (p) “spill from platform”, the generic definition given in (eq.1) becomes the ones given in (eq.2).

$$P_e(l,p) = \frac{S_e(l,p)}{O(l,p)}\ ,\ P_s(l,p) = \frac{S_s(l,p)}{O(l,p)}\ ,\ P_p(l,p) = \frac{S_p(l,p)}{O(l,p)} \qquad \text{(eq. 2)}$$

Where :

- $S_e(l,p)$, $S_s(l,p)$ et $S_p(l,p)$ are the number of occurrences of oil presence detected on a pixel by image-interpretation of -natural leaks (oil seepages), -pollution of boats (oil spill ships) and -pollution of platforms (oil spill platforms) respectively,
- (l,p) are the coordinates (l, p) of the current pixel representing the rows and columns of the image,
- O(l,p) are the number of observation as they appear in the footprints of the processed images Envisat ASAR WSM,

The total probability of presence of oil X per pixel ($P_t(l,p)$) is equal to:

$$P_t(l,p) = \frac{S_e(l,p)}{O(l,p)} + \frac{S_s(l,p)}{O(l,p)} + \frac{S_p(l,p)}{O(l,p)} \qquad \text{(eq. 3)}$$

Thus, we denote by $\hat{A}_X$ the mean area covered in oil of origin X in the Gulf of Guinea between 2002 and 2012. This mean area is given by (eq.4).

$$A_X = \sum_{GG}^{l}\sum_{GG}^{p}(P_X(l,p)\times A(l,p)) \approx \sum_{GG}^{l}\sum_{GG}^{p}(P_X(l,p))\times \overline{A} \qquad \text{(eq. 4)}$$

Where:

- A(l,p) is the area of the pixel (l,p),
- Ā is the mean area of a pixel. Due to the chosen geographic coordinate reference system (CRS), the variation of the area of the pixel (75 m x 75 m) is less than 2.5 % over the Gulf of Guinea (GG).

For a given year Y, the mean area covered in oil of origin X ($\hat{A}_{X,Y}$) is given by (eq.5).

$$A_{X,Y} = \sum_{GG}^{l} \sum_{GG}^{p} (P_{X,Y}(l,p)) \times \overline{A} \qquad \text{(eq. 5)}$$

Where:

- $P_{X,Y}(l,p)$ is the probability of presence of oil of origin X for a given year Y for a given pixel (l,p).

For a given year Y and for a given EEZ, the mean area covered in oil of origin X ($\hat{A}_{X,Y,EEZ}$) is given by (eq.6).

$$A_{X,Y,EEZ} = \sum_{EEZ}^{l} \sum_{EEZ}^{p} (P_{X,Y}(l,p)) \times \overline{A} \qquad \text{(eq. 6)}$$

4.5. Mean fraction covered by oil for a given EEZ

For each country's EEZ over a given period of time, we estimated the mean fraction covered in oil of origin X and for a given year Y ($P_{X,Y,EEZ}$) by dividing the mean area covered in oil of origin X for a given year Y for a given EEZ ($\hat{A}_{X,Y,EEZ}$) by the area of the country's EEZ A_{EEZ} (eq.7). When presenting the results, the term EEZ was replaced by the country's ISO code.

$$P_{X,Y,EEZ} = \frac{A_{X,Y,EEZ}}{A_{EEZ}} \qquad \text{(eq. 7)}$$

5. Results and discussion

5.1. Spatial distribution of oil slicks in the Gulf of Guinea

The spatial and temporal analysis on the Gulf of Guinea allowed the image-interpretation of 18,063 oil slicks. The database of the 18,063 identified objects includes two classes of mineral oil. On the one hand, anthropogenic pollution that come from oil spill platforms and recurring deballasting of oil spill ships. On the other hand, natural oil seepage resurgences which are hints of the presence of hydrocarbon reservoirs in the sub-surface of the Gulf of Guinea.

The fig. 10 illustrates the spatial distribution of the 18,063 oil slicks that have been detected and then mapped in the Gulf of Guinea over the period 2002-2012. For each of the N slicks, a point has been designated as the source, forming a discrete dot map. In order to obtain a continuous density map, each source point of this dot map has been convoluted by a 2-D kernel function. In fact, the density map is the sum of each of these N kernel functions The fig. 11, fig. 12, and fig. 13 respectively show the density maps of oil seepages, spill from ships and spill from platforms. The kernel function that has been used is:

$$K(r)=(1-(r/0.7)^2)^2 \text{ if } r<=0.7$$
$$K(r)=0 \text{ if } r>0.7° \qquad \text{(eq. 8)}$$

Where r is the Euclidian distance to the source point in degrees.

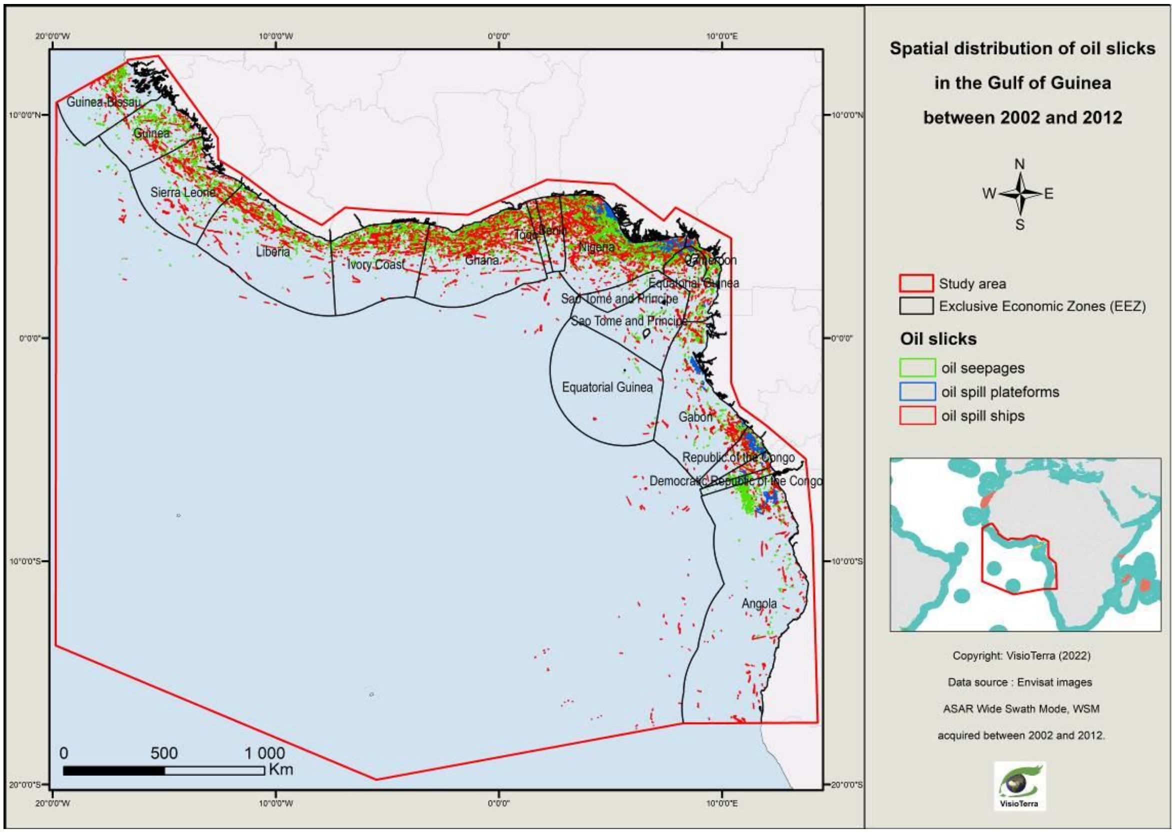

fig. 10 - Spatial distribution of oil slicks in the Gulf of Guinea between 2002 and 2012.

The fig. 11 shows that oil seepages are distributed over all the EEZs in the Gulf of Guinea. This large amount of oil seepages from the Gulf of Guinea could be partly explained by its geology resulting from the opening of the South Atlantic domain initiated in the Lower Cretaceous and by the significant sediment supply from the Niger Delta (Grimaud et al., 2018).

The proximity of the main maritime routes to the coasts contributes to the concentration of discharges in these places. This phenomenon is especially noticed along the coasts of Nigeria which is one of the main shipping routes and occupies a place in maritime piracy (see fig. 12). Thus, there are significant spills of ships there, despite the international convention for the prevention of pollution from ships (MARPOL 73/78), which came into force in 1983. Illegal dumping operations include deballasting and cleaning of ship tanks.

Offshore oil platforms have been found all along the coasts of the EEZs of the top oil producing countries (Nigeria, Angola, Republic of Congo, Ghana...) in the Gulf of Guinea (see fig. 13). The oil spills coming from platforms that have been observed in our study are very well correlated with offshore installations.

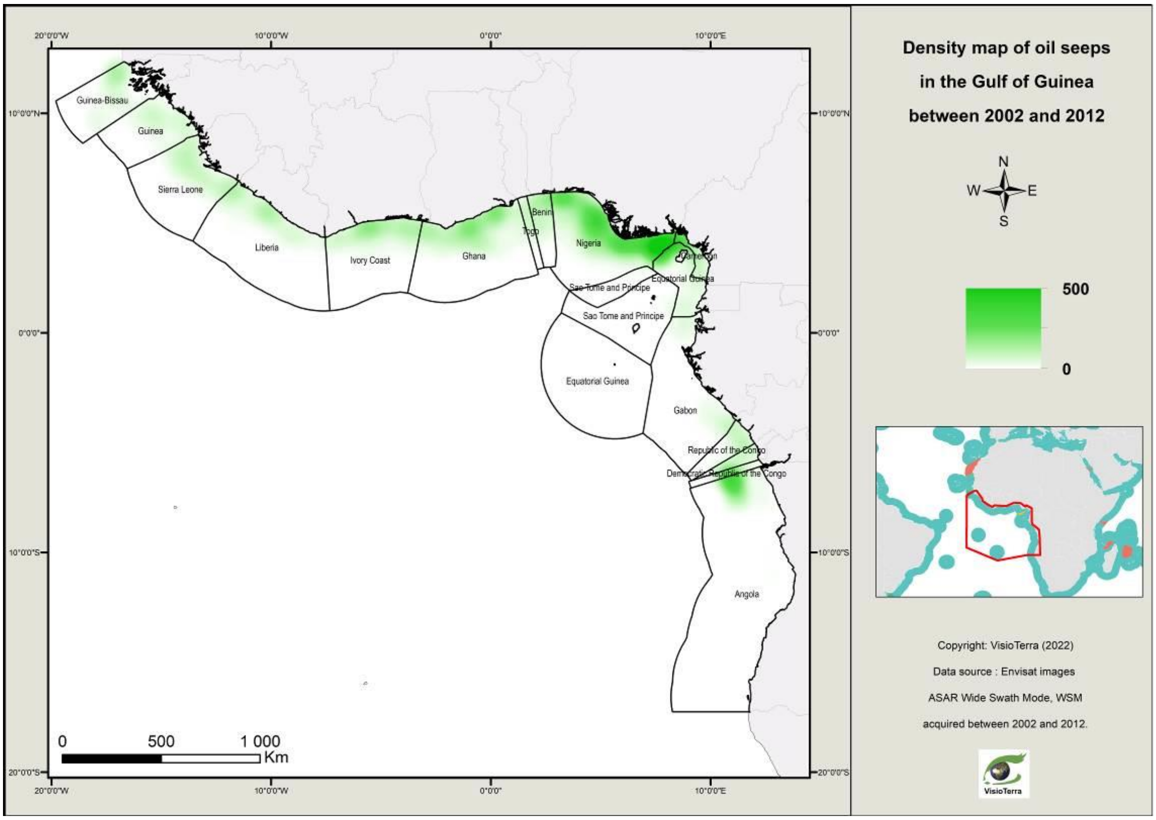

fig. 11 - Density map of oil seeps in the Gulf of Guinea between 2002 and 2012.

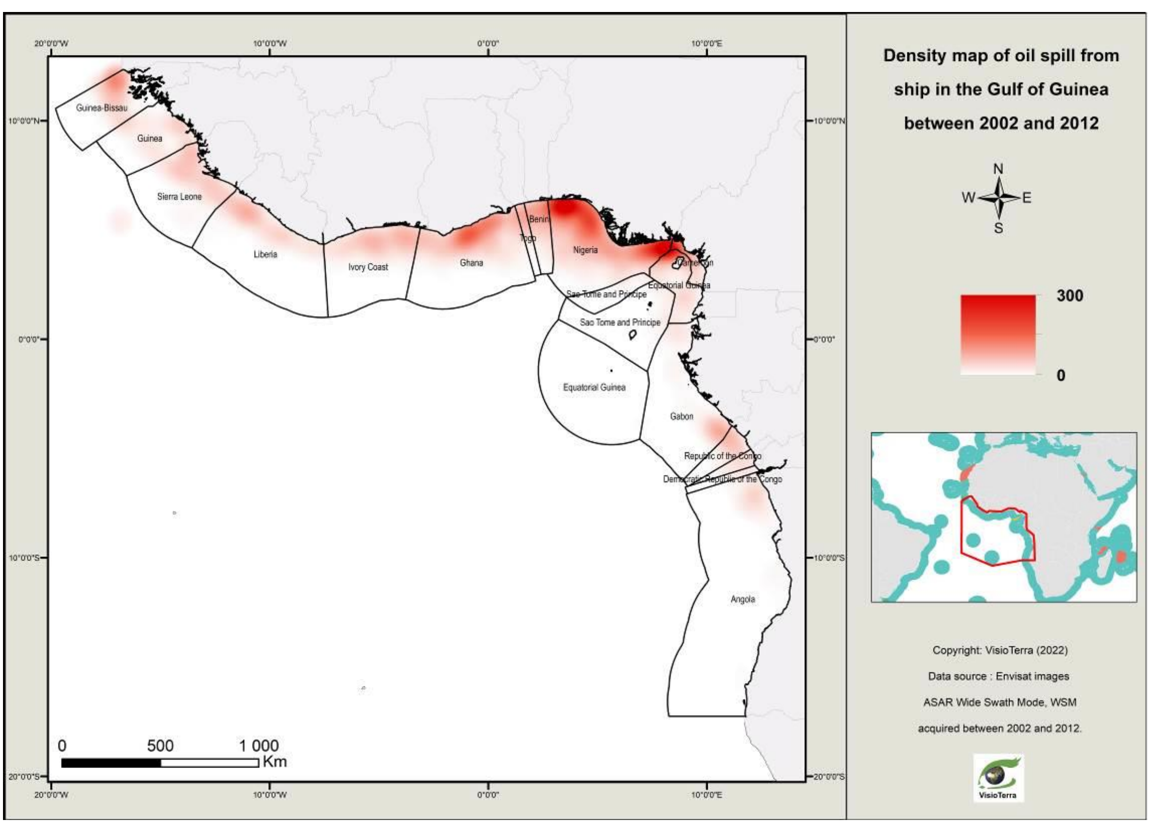

fig. 12 - Density map of oil spill from ship in the Gulf of Guinea between 2002 and 2012.

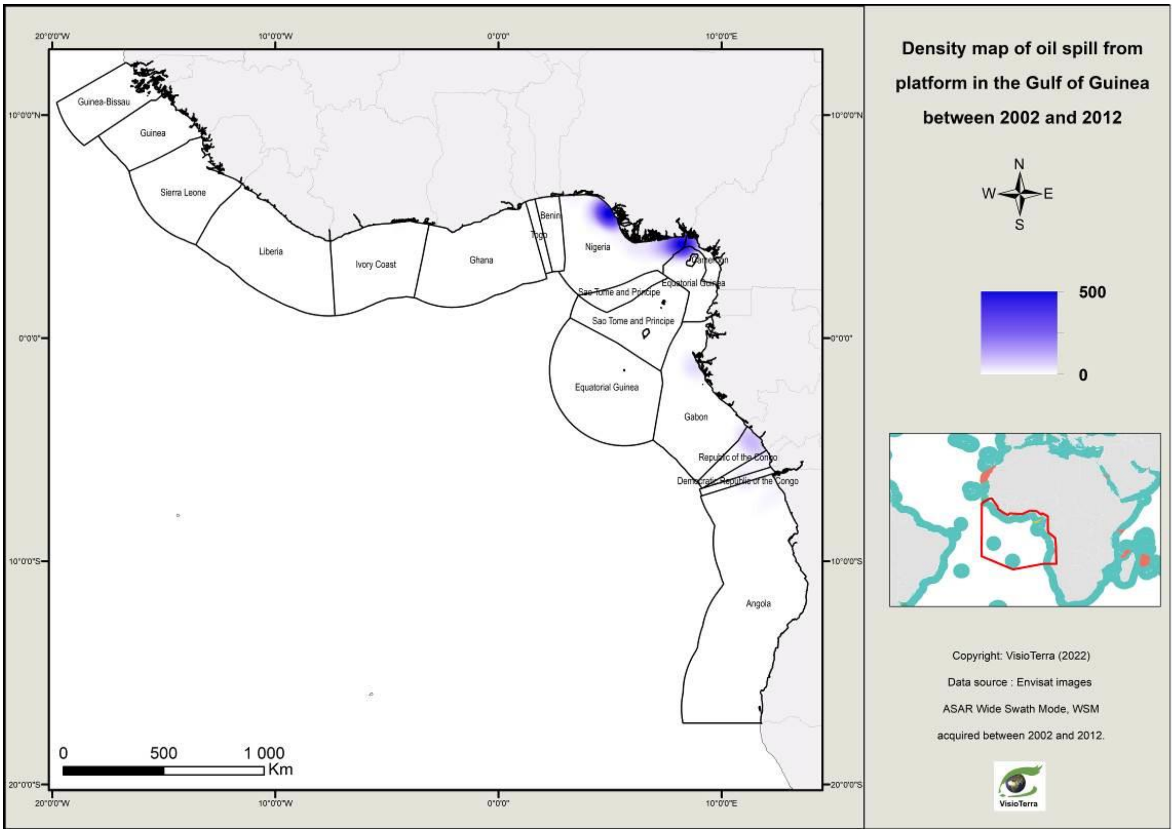

fig. 13 - Density map of oil spill from platforms in the Gulf of Guinea between 2002 and 2012.

5.2. Mean area covered in oil ($\hat{A}_{X,Y,EEZ}$)

5.2.1. Mean area covered in oil in the Gulf of Guinea ($\hat{A}_{X,Y}$)

The fig. 14 shows the mean area covered in oil in the Gulf of Guinea by year. One may notice that:

- the mean area covered in oil slicks from natural origin (oil seeps) remains more or less stable during the period 2002-2012,
- the mean area covered with oil slicks from oil spill platforms seems to have increased significantly during 2008 and then returned to normal in 2009 until the end of the study period,
- the mean area covered in oil slicks from ships seems to have increased after 2004 with a peak between 2007 and 2008, then have fallen in 2009 and remained stable until the end of the study period.

The mean area covered with oil slicks over the entire Gulf of Guinea (GG) between 2002 and 2012 is 145 km² for oil seeps, 111 km² for oil spills from platform and 308 km², oil spills from ship and 547 km² for all oil slicks (table 1). That means that we have detected an oil slick area of 574 km² for a per “full-coverage observation” during 2002-2012. This result is very similar to the one obtained by Dong et al. (2022) that detects an oil slick area of 568 km² for a per “full-coverage observation” during 2014-2019 using Sentinel-1 data.

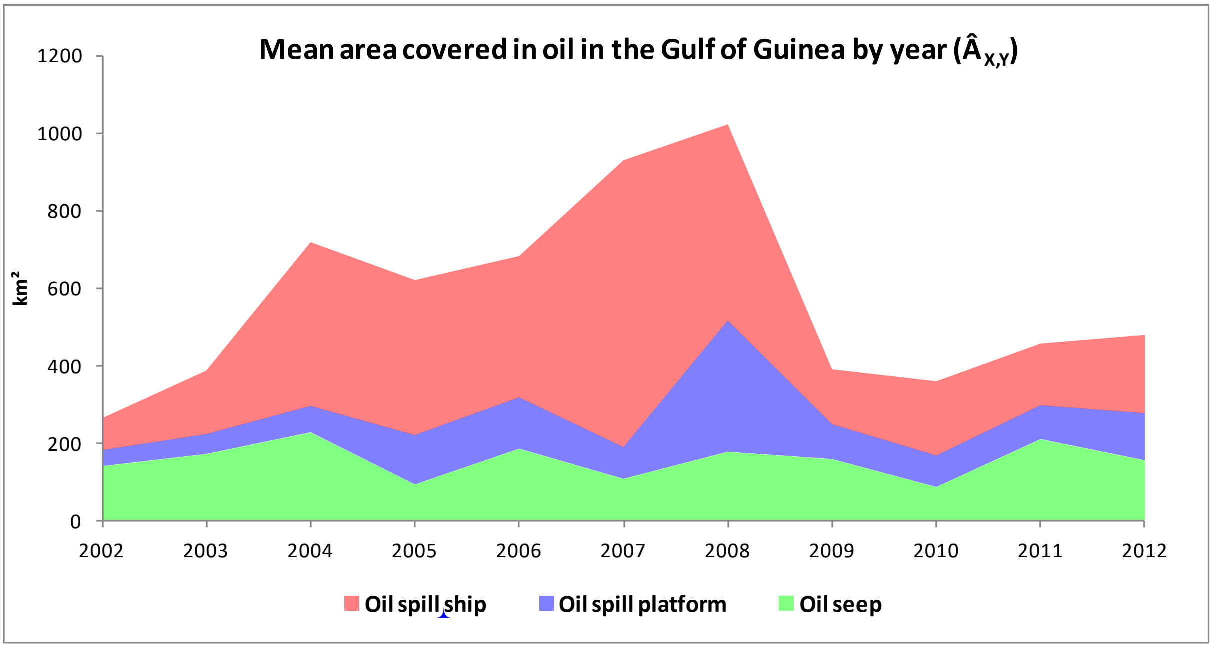

fig. 14 - Mean area covered in oil in the Gulf of Guinea by year ($\hat{A}_{X,Y}$).

Oil slicks	**Mean area covered in oil in GG**
Oil seep	154 km²
Oil spill from platform	111 km²
Oil spill from ship	308 km²
Total	**574** km²

table 1 – Temporal mean of the yearly mean area covered in oil in the Gulf of Guinea between 2002 and 2012.

5.2.2. Mean area covered in oil by EEZ of country ($\hat{A}_{X,Y,EEZ}$)

The fig. 15 shows the mean area covered in oil by EEZ of countries between 2002 and 2012. The fig. 16 shows the mean area covered in oil by EEZ of countries by year. One may notice that the most polluted EEZ are Nigeria followed by Angola, Republic of Congo and Cameroon.

The analysis by EEZ shows that the decrease in oil spills observed between 2008 and 2009 (fig. 14) was driven by the major oil producing countries: Angola, Nigeria and Republic of Congo (fig. 16).

The fall in the mean area covered in oil from platforms and ships may be explained by the economic crisis of 2008. In fact, 2008 world crisis had led to the falling in oil prices inducing deficit in the budget of oil companies and governments. For instance, Angola oil production decreased in 2009 following the post-2008 slowdown in global economic activity and the subsequent glut of oil on the global market (Mikidadu, 2018).

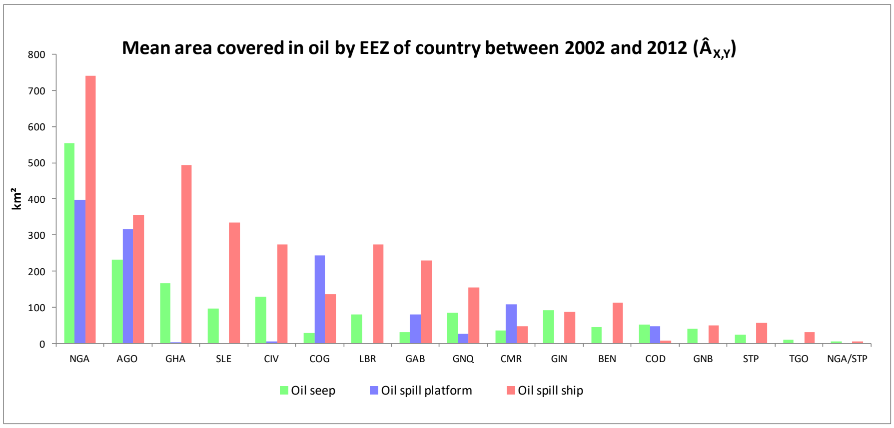

fig. 15 - Mean area covered in oil by EEZ of country ($\hat{A}_{X,Y}$) between 2002 and 2012.

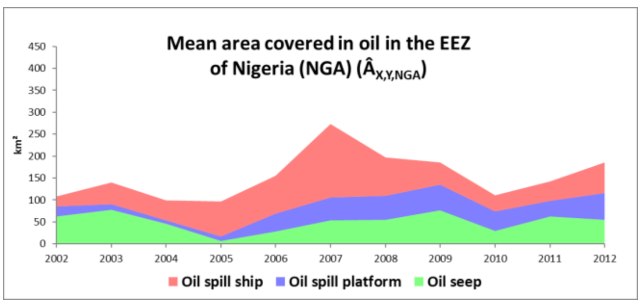

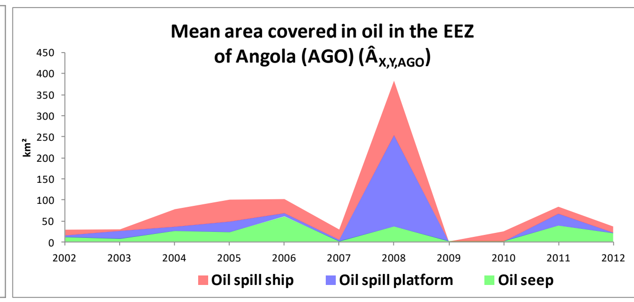

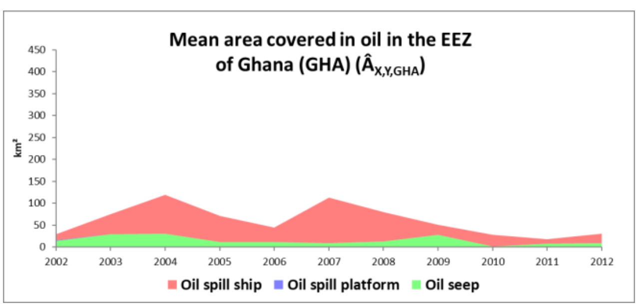

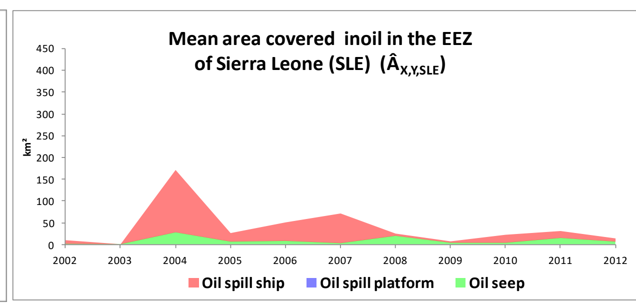

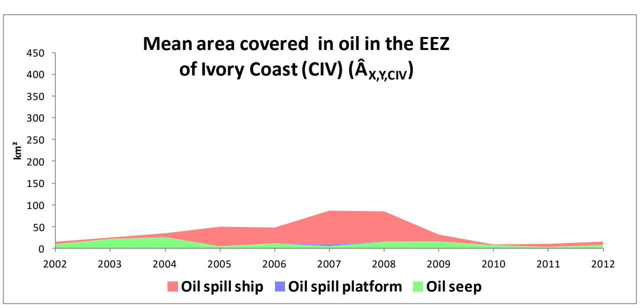

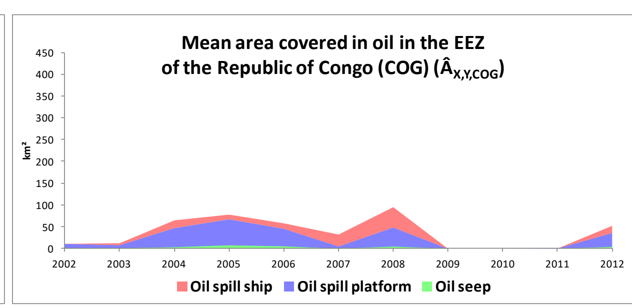

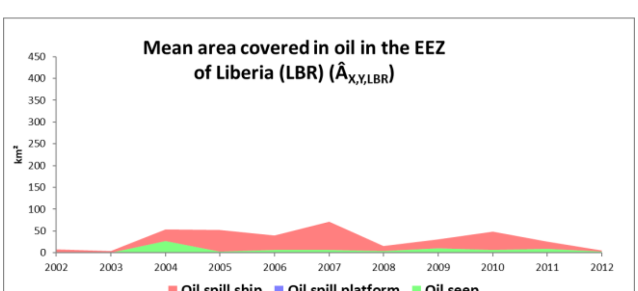

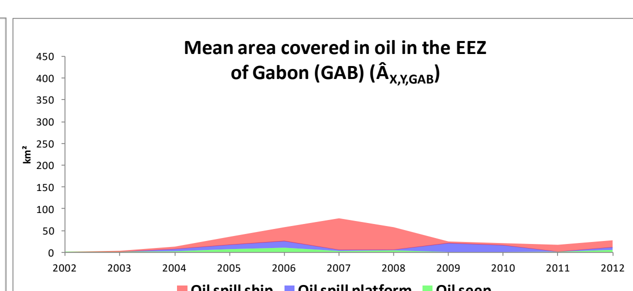

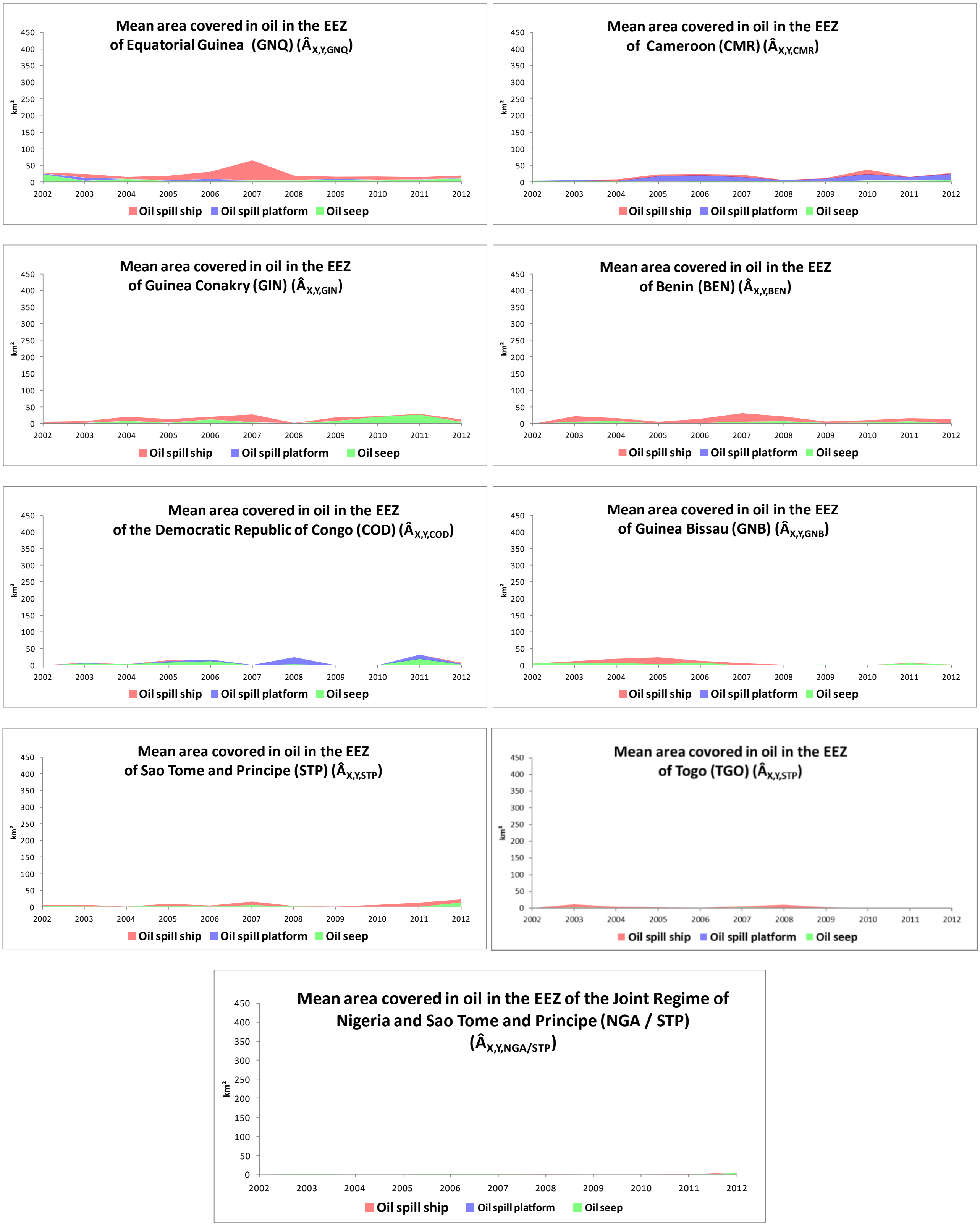

fig. 16 - Mean area covered in oil by EEZ of countries per year ($\hat{A}_{X,Y,EEZ}$).

5.3. *Mean fraction covered by oil by EEZ (* $P_{X,Y,EEZ}$ *)*

As shown in fig.15, Nigeria holds the record for pollution by platforms and also by boats. These data incorporated the pollution observed throughout its whole EEZ. But isn't it also because Nigeria has an extended EEZ? To make the analysis independent of the size of the EEZ, we calculate the "Mean fraction covered by oil by EEZ".

The fig. 17 shows the mean fraction covered by oil by EEZ of countries between 2002 and 2012. The fig. 18 shows the mean fraction covered by oil by EEZ of countries by year.

The country mean fraction covered by oil which divides the mean area covered in oil by the country EEZ area (eq.7) gives an idea of the mean probability to be covered by oil by EEZ. Thus, the largest the mean fraction is, the more the area is likely to be covered by it. One may see that the probability that an oil spill occurs is high for the Republic of Congo, Cameroon and Nigeria while the probability that an oil seep occurs is high for the Democratic Republic of the Congo, Nigeria and Cameroon.

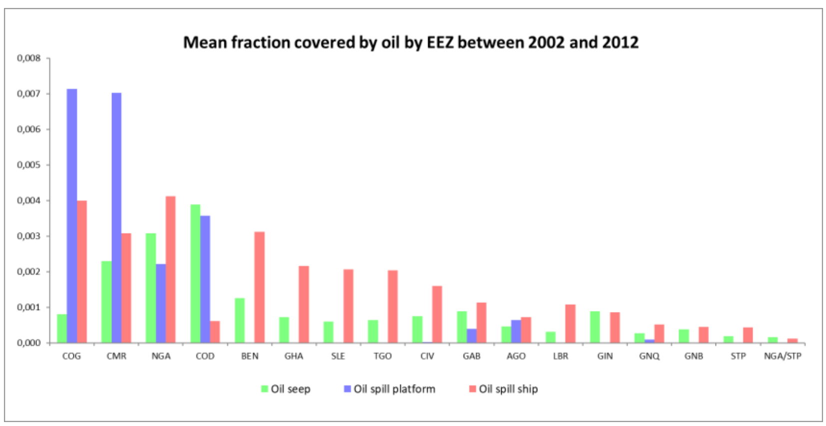

fig. 17 - Mean fraction covered by spilled oil by EEZ between 2002 and 2012.

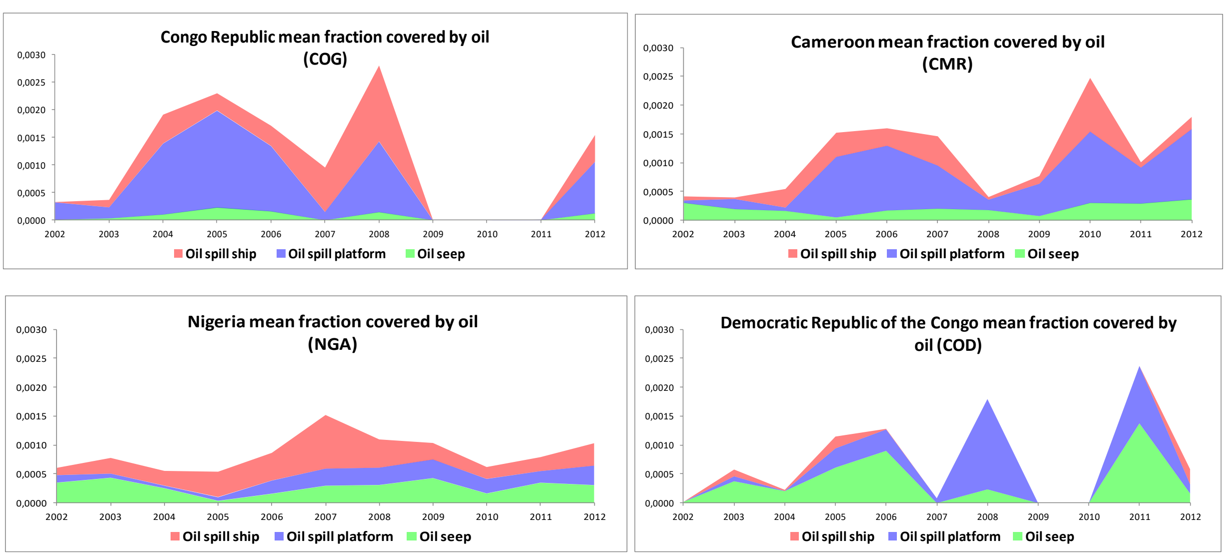

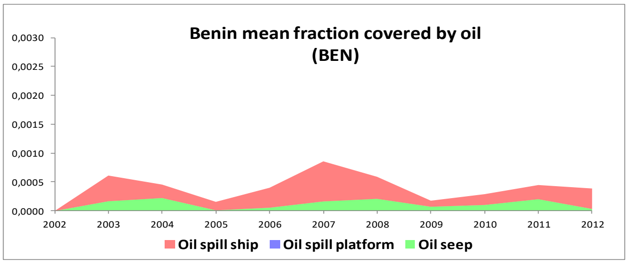
Benin mean fraction covered by oil
(BEN)
0,0030
0,0025
0,0020
0,0015
0,0010
0,0005
0,0000
2002 2003 2004 2005 2006 2007 2008 2009 2010 2011 2012
Oil spill ship
Oil spill platform
Oil seep

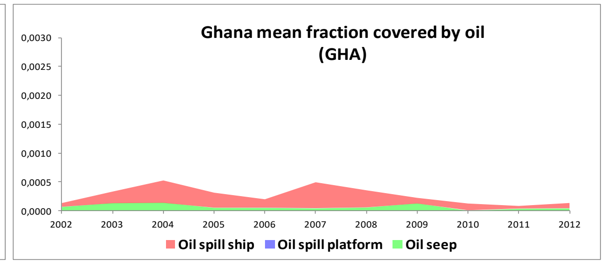
Ghana mean fraction covered by oil
(GHA)
0,0030
0,0025
0,0020
0,0015
0,0010
0,0005
0,0000
2002 2003 2004 2005 2006 2007 2008 2009 2010 2011 2012
Oil spill ship
Oil spill platform
Oil seep

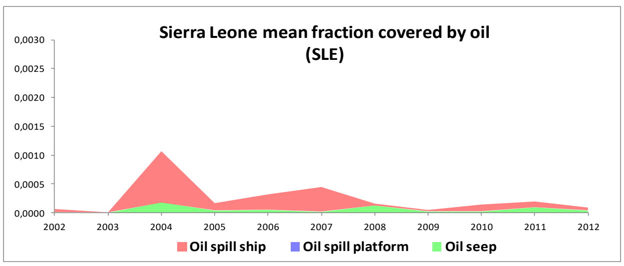
Sierra Leone mean fraction covered by oil
(SLE)
0,0030
0,0025
0,0020
0,0015
0,0010
0,0005
0,0000
2002 2003 2004 2005 2006 2007 2008 2009 2010 2011 2012
Oil spill ship
Oil spill platform
Oil seep

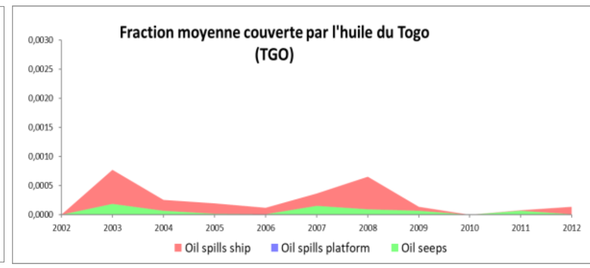
Fraction moyenne couverte par l'huile du Togo
(TGO)
0,0030
0,0025
0,0020
0,0015
0,0010
0,0005
0,0000
2002 2003 2004 2005 2006 2007 2008 2009 2010 2011 2012
Oil spills ship
Oil spills platform
Oil seeps

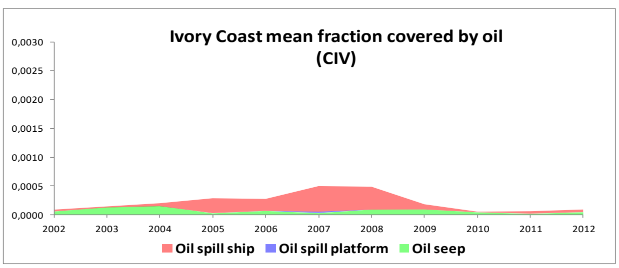
Ivory Coast mean fraction covered by oil
(CIV)
0,0030
0,0025
0,0020
0,0015
0,0010
0,0005
0,0000
2002 2003 2004 2005 2006 2007 2008 2009 2010 2011 2012
Oil spill ship
Oil spill platform
Oil seep

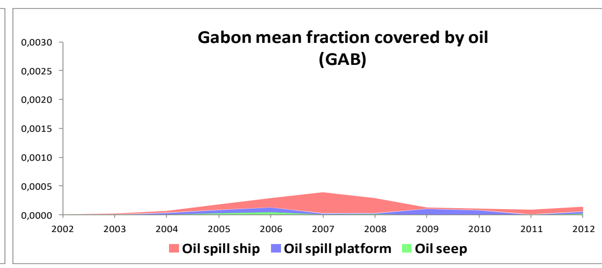
Gabon mean fraction covered by oil
(GAB)
0,0030
0,0025
0,0020
0,0015
0,0010
0,0005
0,0000
2002 2003 2004 2005 2006 2007 2008 2009 2010 2011 2012
Oil spill ship
Oil spill platform
Oil seep

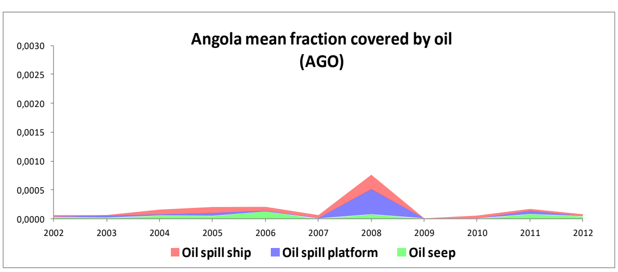
Angola mean fraction covered by oil
(AGO)
0,0030
0,0025
0,0020
0,0015
0,0010
0,0005
0,0000
2002 2003 2004 2005 2006 2007 2008 2009 2010 2011 2012
Oil spill ship
Oil spill platform
Oil seep

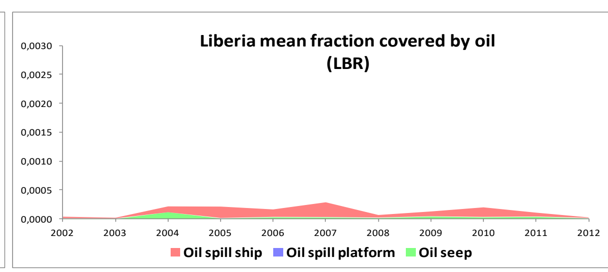
Liberia mean fraction covered by oil
(LBR)
0,0030
0,0025
0,0020
0,0015
0,0010
0,0005
0,0000
2002 2003 2004 2005 2006 2007 2008 2009 2010 2011 2012
Oil spill ship
Oil spill platform
Oil seep

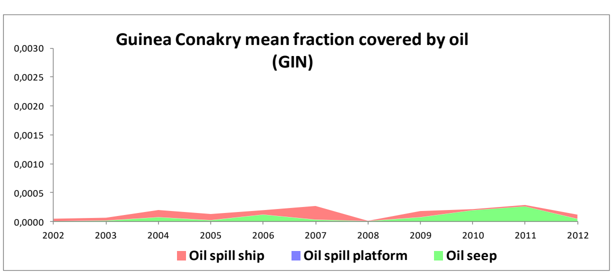
Guinea Conakry mean fraction covered by oil
(GIN)
0,0030
0,0025
0,0020
0,0015
0,0010
0,0005
0,0000
2002 2003 2004 2005 2006 2007 2008 2009 2010 2011 2012
Oil spill ship
Oil spill platform
Oil seep

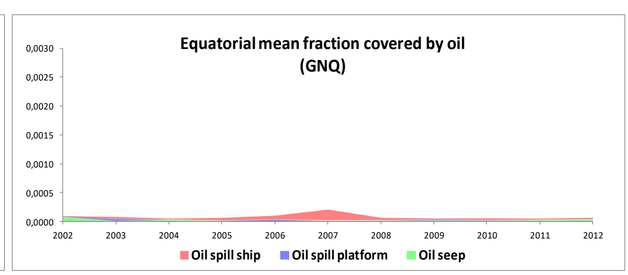
Equatorial mean fraction covered by oil
(GNQ)
0,0030
0,0025
0,0020
0,0015
0,0010
0,0005
0,0000
2002 2003 2004 2005 2006 2007 2008 2009 2010 2011 2012
Oil spill ship
Oil spill platform
Oil seep

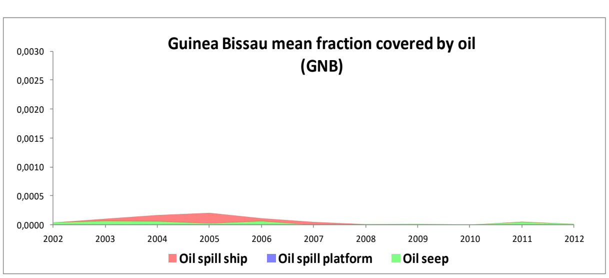
Guinea Bissau mean fraction covered by oil
(GNB)
0,0030
0,0025
0,0020
0,0015
0,0010
0,0005
0,0000
2002 2003 2004 2005 2006 2007 2008 2009 2010 2011 2012
Oil spill ship
Oil spill platform
Oil seep

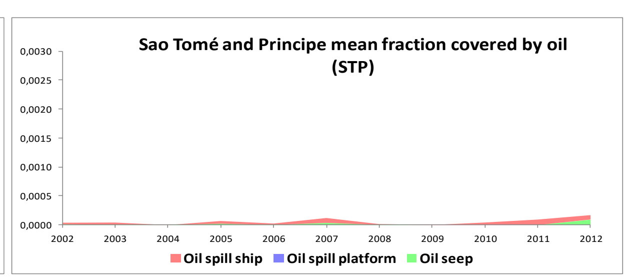
Sao Tomé and Principe mean fraction covered by oil
(STP)
0,0030
0,0025
0,0020
0,0015
0,0010
0,0005
0,0000
2002 2003 2004 2005 2006 2007 2008 2009 2010 2011 2012
Oil spill ship
Oil spill platform
Oil seep

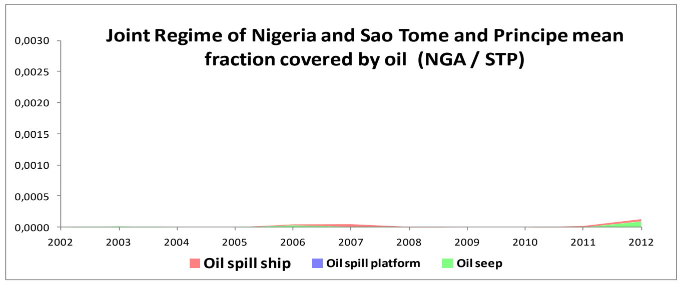

fig. 18 - Mean fraction covered by oil by EEZ by year.

6. Data availability

All the Envisat ASAR images (2002-2012) used in this study are available at ESA website https://eocat.esa.int/sec/#data-services-area. These data can also be viewed on the HEDAVI (Heritage Data Visualization) portal managed by VisioTerra at the address http://hedavi.esa.int/. The spatial distribution of the oil slicks in the Gulf of Guinea between 2002 and 2012 is available at ZENODO: https://doi.org/10.5281/zenodo.6470470 (Najoui, 2022).

A set of 100 georeferenced oil spills is available at ZENODO: https://doi.org/10.5281/zenodo.6907743.

7. Conclusion and perspectives

An unprecedented database of oil spills has been generated over the EEZ of the Gulf of Guinea using the 11 years of acquisitions of SAR images at C-band by ASAR in wide-swath mode (150 m of spatial resolution) contained in the archive of the Envisat mission. This database has been achieved using a manual approach. The present study shows that all of the countries EEZ are sites of natural oil seepages due to the extensive geological context of the Gulf of Guinea. It shows also that oil spills from ships are well correlated to the shipping routes along the coasts of the 17 EEZ of the Gulf of Guinea while oil spills coming from oil platforms are concentrated along the coasts of oil-producing countries like Nigeria, Republic of Congo, Angola, and Ghana. The temporal analysis during 10 years (2002-2012) shows a decrease in the mean area covered by oil between 2008 and 2009. This decreas~~ing~~ is likely to be due to the post-2008 global economic slowdown.

Oil seepages and oil spills monitoring will benefit from Sentinel-1 mission, launched in 2014, owing to its higher spatial resolution (10 m), its temporal resolution (6 days), and its longer period of acquisitions (beyond 2032). This dataset will offer more reliable and timely information for emergency and mitigation policies.

Acknowledgments

The authors would like to thank the ESA (European Spatial Agency) for providing the SAR scenes used in this study.

REFERENCES

Adelana, S., Adeosun, T., 2011. Environmental pollution and remediation: challenges and management of oil Spillage in the Nigerian coastal areas. Am. J. Sci. Ind. Res. 2, 834–845. https://doi.org/10.5251/ajsir.2011.2.6.834.845

Albakjaji, M., 2010. La pollution de la mer méditerranée par les hydrocarbures liée au trafic maritime.

Alpers, W., Holt, B., Zeng, K., 2017. Oil spill detection by imaging radars: Challenges and pitfalls. Remote Sens. Environ. 201, 133–147. https://doi.org/10.1016/j.rse.2017.09.002

Bagby, S.C., Reddy, C.M., Aeppli, C., Fisher, G.B., Valentine, D.L., 2017. Persistence and biodegradation of oil at the ocean floor following *Deepwater Horizon*. Proc. Natl. Acad. Sci. 114, E9–E18. https://doi.org/10.1073/pnas.1610110114

Brekke, C., Solberg, A.H.S., 2008. Classifiers and Confidence Estimation for Oil Spill Detection in ENVISAT ASAR Images. IEEE Geosci. Remote Sens. Lett. 5, 65–69. https://doi.org/10.1109/LGRS.2007.907174

Brekke, C., Solberg, A.H.S., 2005. Oil spill detection by satellite remote sensing. Remote Sens. Environ. 95, 1–13. https://doi.org/10.1016/j.rse.2004.11.015

Caruso, M., Migliaccio, M., Hargrove, J., Garcia-Pineda, O., Graber, H., 2013. Oil Spills and Slicks Imaged by Synthetic Aperture Radar. Oceanography 26. https://doi.org/10.5670/oceanog.2013.34

Chalghmi, H., 2015. Etude de la pollution marine par les hydrocarbures et caractérisation de leurs effets biochimiques et moléculaires sur la palourde de Ruditapes sp.

Del Frate, F., Petrocchi, A., Lichtenegger, J., Calabresi, G., 2000. Neural networks for oil spill detection using ERS-SAR data. IEEE Trans. Geosci. Remote Sens. 38, 2282–2287. https://doi.org/10.1109/36.868885

Dong, Y., Liu, Y., Hu, C., MacDonald, I.R., Lu, Y., 2022. Chronic oiling in global oceans. Science 376, 1300–1304. https://doi.org/10.1126/science.abm5940

Espedal, H.A., 1999. Satellite SAR oil spill detection using wind history information. Int. J. Remote Sens. 20, 49–65. https://doi.org/10.1080/014311699213596

Favennec, J.-P., Copinschi, P., Cavatorta, T., Esen, F., 2003. Les nouveaux enjeux pétroliers en Afrique. Polit. Afr. 89, 127. https://doi.org/10.3917/polaf.089.0127

Fingas, M., Brown, C., 2017. A Review of Oil Spill Remote Sensing. Sensors 18, 91. https://doi.org/10.3390/s18010091

Fiscella, B., Giancaspro, A., Nirchio, F., Pavese, P., Trivero, P., 2000. Oil spill detection using marine SAR images. Int. J. Remote Sens. 21, 3561–3566. https://doi.org/10.1080/014311600750037589

Fuhrer, M., 2012. Transport maritime de produits chimiques liquides et flottants : etude experimentale du rejet accidentel sous-marin suite a un naufrage.

Gade, M., Alpers, W., Hühnerfuss, H., Masuko, H., Kobayashi, T., 1998. Imaging of biogenic and anthropogenic ocean surface films by the multifrequency/multipolarization SIR-C/X-SAR. J. Geophys. Res. Oceans 103, 18851–18866. https://doi.org/10.1029/97JC01915

Garcia-Pineda, O., MacDonald, I., Zimmer, B., 2008. Synthetic Aperture Radar Image Processing using the Supervised Textural-Neural Network Classification Algorithm, in: IGARSS 2008 - 2008 IEEE International Geoscience and Remote Sensing Symposium. Presented at the IGARSS 2008 - 2008 IEEE International Geoscience and Remote Sensing Symposium, IEEE, Boston, MA, USA, p. IV-1265-IV–1268. https://doi.org/10.1109/IGARSS.2008.4779960

Grimaud, J.-L., Rouby, D., Chardon, D., Beauvais, A., 2018. Cenozoic sediment budget of West Africa and the Niger delta. Basin Res. 30, 169–186. https://doi.org/10.1111/bre.12248

Jackson, C.R., Apel, J.R., United States (Eds.), 2004. Synthetic aperture radar: marine user's manual. U.S. Dept. of Commerce : National Oceanic and Atmospheric Administration, Washington, D.C.

Jafarzadeh, H., Mahdianpari, M., Homayouni, S., Mohammadimanesh, F., Dabboor, M., 2021. Oil spill detection from Synthetic Aperture Radar Earth observations: a meta-analysis and comprehensive review. GIScience Remote Sens. 58, 1022–1051. https://doi.org/10.1080/15481603.2021.1952542

Jatiault, R., Dhont, D., Loncke, L., Dubucq, D., 2017. Monitoring of natural oil seepage in the Lower Congo Basin using SAR observations. Remote Sens. Environ. 191, 258–272. https://doi.org/10.1016/j.rse.2017.01.031

Johannessen, O.M., Sandven, S., Jenkins, A.D., Durand, D., Pettersson, L.H., Espedal, H., Evensen, G., Hamre, T., 2000. Satellite earth observation in operational oceanography. Coast. Eng. 41, 155–176. https://doi.org/10.1016/S0378-3839(00)00030-2

Kanaa, T.F.N., Tonye, E., Mercier, G., Onana, V.P., Ngono, J.M., Frison, P.L., Rudant, J.P., Garello, R., 2003. Detection of oil slick signatures in SAR images by fusion of hysteresis thresholding responses, in: IGARSS 2003. 2003 IEEE International Geoscience and Remote Sensing Symposium. Proceedings (IEEE Cat. No.03CH37477). Presented at the IGARSS 2003. 2003 IEEE International Geoscience and Remote Sensing Symposium., IEEE, Toulouse, France, pp. 2750–2752. https://doi.org/10.1109/IGARSS.2003.1294573

Khanna, S., Santos, M., Ustin, S., Shapiro, K., Haverkamp, P., Lay, M., 2018. Comparing the Potential of Multispectral and Hyperspectral Data for Monitoring Oil Spill Impact. Sensors 18, 558. https://doi.org/10.3390/s18020558

Kubat, M., Holte, R.C., Matwin, S., 1998. Machine Learning for the Detection of Oil Spills in Satellite Radar Images. Mach. Learn. 30, 195–215. https://doi.org/10.1023/A:1007452223027

Langangen, Ø., Olsen, E., Stige, L.C., Ohlberger, J., Yaragina, N.A., Vikebø, F.B., Bogstad, B., Stenseth, N.C., Hjermann, D.Ø., 2017. The effects of oil spills on marine fish: Implications of spatial variation in natural mortality. Mar. Pollut. Bull. 119, 102–109. https://doi.org/10.1016/j.marpolbul.2017.03.037

Lawrence, S.R., Munday, S., Bray, R., 2002. Regional geology and geophysics of the eastern Gulf of Guinea (Niger Delta to Rio Muni). Lead. Edge 21, 1112–1117. https://doi.org/10.1190/1.1523752

Leifer, I., Lehr, W.J., Simecek-Beatty, D., Bradley, E., Clark, R., Dennison, P., Hu, Y., Matheson, S., Jones, C.E., Holt, B., Reif, M., Roberts, D.A., Svejkovsky, J., Swayze, G., Wozencraft, J., 2012. State of the art satellite and airborne marine oil spill remote sensing: Application to the BP Deepwater Horizon oil spill. Remote Sens. Environ. 124, 185–209. https://doi.org/10.1016/j.rse.2012.03.024

Li, Y., Hu, C., Quigg, A., Gao, H., 2019. Potential influence of the Deepwater Horizon oil spill on phytoplankton primary productivity in the northern Gulf of Mexico. Environ. Res. Lett. 14, 094018. https://doi.org/10.1088/1748-9326/ab3735

Li, Z., Johnson, W., 2019. An Improved Method to Estimate the Probability of Oil Spill Contact to Environmental Resources in the Gulf of Mexico. J. Mar. Sci. Eng. 7, 41. https://doi.org/10.3390/jmse7020041

Liu, A.K., Peng, C.Y., Chang, S.Y.-S., 1997. Wavelet analysis of satellite images for coastal watch. IEEE J. Ocean. Eng. 22, 9–17. https://doi.org/10.1109/48.557535

Louet, J., Bruzzi, S., 1999. ENVISAT mission and system, in: IEEE 1999 International Geoscience and Remote Sensing Symposium. IGARSS'99 (Cat. No.99CH36293). IEEE, Hamburg, Germany, pp. 1680–1682. https://doi.org/10.1109/IGARSS.1999.772059

MacDonald, I.R., Garcia-Pineda, O., Beet, A., Daneshgar Asl, S., Feng, L., Graettinger, G., French-McCay, D., Holmes, J., Hu, C., Huffer, F., Leifer, I., Muller-Karger, F., Solow, A., Silva, M., Swayze, G., 2015. Natural and unnatural oil slicks in the G ulf of M exico. J. Geophys. Res. Oceans 120, 8364–8380. https://doi.org/10.1002/2015JC011062

Marghany, M., 2015. Automatic detection of oil spills in the Gulf of Mexico from RADARSAT-2 SAR satellite data. Environ. Earth Sci. 74, 5935–5947. https://doi.org/10.1007/s12665-015-4617-y

Mercier, G., Girard-Ardhuin, F., 2006. Partially Supervised Oil-Slick Detection by SAR Imagery Using Kernel Expansion. IEEE Trans. Geosci. Remote Sens. 44, 2839–2846. https://doi.org/10.1109/TGRS.2006.881078

Mfewou, A., Tchekote, H., Lemouogue, J., 2018. Frontières Et Dynamiques Socio-Spatiales En Afrique : Une Analyse À Partir Des Frontières Sud- Camerounaises. Eur. Sci. J. ESJ 14, 285. https://doi.org/10.19044/esj.2018.v14n5p285

Mikidadu, M., 2018. Oil Production and Economic Growth in Angola. Int. J. Energy Econ. Policy 8, 127–131.

Miranda, N., Rosich, B., Meadows, P.J., Haria, K., Small, D., Schubert, A., Lavalle, M., Collard, F., Johnsen, H., Monti-Guarnieri, A., D'Aria, D., 2013. The Envisat ASAR mission: A look back at 10 years of operation. https://doi.org/10.5167/UZH-96146

NAE-NRC, 2012. Macondo Well Deepwater Horizon Blowout: Lessons for Improving Offshore Drilling Safety. National Academies Press, Washington, D.C. https://doi.org/10.17226/13273

Najoui, Z., 2022. Spatial distribution of oil slicks in the Gulf of Guinea between 2002 and 2012. Zenodo. https://doi.org/10.5281/ZENODO.6470470

Najoui, Z., 2017. Prétraitement optimal des images radar et modélisation des dérives de nappes d'hydrocarbures pour l'aide à la photo-interprétation en exploration pétrolière et surveillance environnementale.

Najoui, Z., Riazanoff, S., Deffontaines, B., Xavier, J.-P., 2018a. Estimated location of the seafloor sources of marine natural oil seeps from sea surface outbreaks: A new "source path procedure" applied to the northern Gulf of Mexico. Mar. Pet. Geol. 91, 190–201. https://doi.org/10.1016/j.marpetgeo.2017.12.035

Najoui, Z., Riazanoff, S., Deffontaines, B., Xavier, J.-P., 2018b. A Statistical Approach to Preprocess and Enhance C-Band SAR Images in Order to Detect Automatically Marine Oil Slicks. IEEE Trans. Geosci. Remote Sens. 56, 2554–2564. https://doi.org/10.1109/TGRS.2017.2760516

Ngodi, E., 2005. Gestion des ressources pétrolières et développement en Afrique.

Okafor-Yarwood, I., 2018. The effects of oil pollution on the marine environment in the Gulf of Guinea—the Bonga Oil Field example. Transnatl. Leg. Theory 9, 254–271. https://doi.org/10.1080/20414005.2018.1562287

Ovadia, J.S., 2016. The petro-developmental state in Africa: making oil work in Angola, Nigeria and the Gulf of Guinea. Hurst & Company, London.

Pinkston, F.W.M., Flemings, P.B., 2019. Overpressure at the Macondo Well and its impact on the Deepwater Horizon blowout. Sci. Rep. 9, 7047. https://doi.org/10.1038/s41598-019-42496-0

Reuscher, M.G., Baguley, J.G., Montagna, P.A., 2020. The expanded footprint of the Deepwater Horizon oil spill in the Gulf of Mexico deep-sea benthos. PLOS ONE 15, e0235167. https://doi.org/10.1371/journal.pone.0235167

Scheren, P.A., Ibe, A.C., Janssen, F.J., Lemmens, A.M., 2002. Environmental pollution in the Gulf of Guinea – a regional approach. Mar. Pollut. Bull. 44, 633–641. https://doi.org/10.1016/S0025-326X(01)00305-8

Shu, Y., Li, J., Yousif, H., Gomes, G., 2010. Dark-spot detection from SAR intensity imagery with spatial density thresholding for oil-spill monitoring. Remote Sens. Environ. 114, 2026–2035. https://doi.org/10.1016/j.rse.2010.04.009

Solberg, A.H.S., Storvik, G., Solberg, R., Volden, E., 1999. Automatic detection of oil spills in ERS SAR images. IEEE Trans. Geosci. Remote Sens. 37, 1916–1924. https://doi.org/10.1109/36.774704

Suresh, G., Melsheimer, C., Korber, J.-H., Bohrmann, G., 2015. Automatic Estimation of Oil Seep Locations in Synthetic Aperture Radar Images. IEEE Trans. Geosci. Remote Sens. 53, 4218–4230. https://doi.org/10.1109/TGRS.2015.2393375

The ENVISAT Mission and System, n.d.

Trivero, P., Biamino, W., 2010. Observing Marine Pollution with Synthetic Aperture Radar, in: Imperatore, P., Riccio, D. (Eds.), Geoscience and Remote Sensing New Achievements. InTech. https://doi.org/10.5772/9106

Tull, D.M., 2008. Oil and Politics in the Gulf of Guinea by Ricardo Soares de Oliveira London: Hurst & Co/New York: Columbia University Press, 2007. Pp. 379. £20.00 (pb). J. Mod. Afr. Stud. 46, 692–694. https://doi.org/10.1017/S0022278X08003558

Xu, L., Shafiee, M.J., Wong, A., Li, F., Wang, L., Clausi, D., 2015. Oil spill candidate detection from SAR imagery using a thresholding-guided stochastic fully-connected conditional random field model, in: 2015 IEEE Conference on Computer Vision and Pattern

Recognition Workshops (CVPRW). Presented at the 2015 IEEE Conference on Computer Vision and Pattern Recognition Workshops (CVPRW), IEEE, Boston, MA, USA, pp. 79–86. https://doi.org/10.1109/CVPRW.2015.7301386

Yaghmour, F., Els, J., Maio, E., Whittington-Jones, B., Samara, F., El Sayed, Y., Ploeg, R., Alzaabi, A., Philip, S., Budd, J., Mupandawana, M., 2022. Oil spill causes mass mortality of sea snakes in the Gulf of Oman. Sci. Total Environ. 825, 154072. https://doi.org/10.1016/j.scitotenv.2022.154072

Zhang, Y., Li, Y., Lin, H., 2014. Oil-Spill Pollution Remote Sensing by Synthetic Aperture Radar, in: Marghany, M. (Ed.), Advanced Geoscience Remote Sensing. InTech. https://doi.org/10.5772/57477